AEDC-TR-76-158

cy. 2

1977

DEC 2 0

MAY 1 8 1982

JAN 2

AN APPLICATION OF THE CHAPMAN-KORST THEORY TO SUPERSONIC NOZZLE-AFTERBODY FLOWS

ENGINE TEST FACILITY
ARNOLD ENGINEERING DEVELOPMENT CENTER
AIR FORCE SYSTEMS COMMAND
ARNOLD AIR FORCE STATION, TENNESSEE 37389

January 1977

Final Report for Period July 1, 1975 to September 30, 1976

Approved for public release; distribution unlimited.

Property of U. S. Air Force
AEDC LIBRARY
F40600-75-C 0001

Prepared for

DIRECTORATE OF TECHNOLOGY (DY)
ARNOLD ENGINEERING DEVELOPMENT CENTER
ARNOLD AIR FORCE STATION, TENNESSEE 37389

NOTICES

When U. S. Government drawings specifications, or other data are used for any purpose other than a definitely related Government procurement operation, the Government thereby incurs no responsibility nor any obligation whatsoever, and the fact that the Government may have formulated, furnished, or in any way supplied the said drawings, specifications, or other data, is not to be regarded by implication or otherwise, or in any manner licensing the holder or any other person or corporation, or conveying any rights or permission to manufacture, use, or sell any patented invention that may in any way be related thereto.

Qualified users may obtain copies of this report from the Defense Documentation Center.

References to named commercial products in this report are not to be considered in any sense as an endorsement of the product by the United States Air Force or the Government.

This report has been reviewed by the Information Office (OI) and is releasable to the National Technical Information Service (NTIS). At NTIS, it will be available to the general public, including foreign nations.

APPROVAL STATEMENT

This technical report has been reviewed and is approved for publication.

FOR THE COMMANDER

Elton R. Thompson

ELTON R. THOMPSON
Research & Development
Division
Directorate of Technology

Robert O. Dietz

ROBERT O. DIETZ
Director of Technology

UNCLASSIFIED

REPORT DOCUMENTATION PAGE		READ INSTRUCTIONS BEFORE COMPLETING FORM
1 REPORT NUMBER AEDC-TR-76-158	2 GOVT ACCESSION NO.	3 RECIPIENT'S CATALOG NUMBER
4 TITLE (and Subtitle) AN APPLICATION OF THE CHAPMAN-KORST THEORY TO SUPERSONIC NOZZLE-AFTERBODY FLOWS		5 TYPE OF REPORT & PERIOD COVERED Final Report-July 1, 1975 to September 30, 1976 6. PERFORMING ORG. REPORT NUMBER
7 AUTHOR(s) R. C. Bauer and J. H. Fox, ARO, Inc.		8. CONTRACT OR GRANT NUMBER(s)
9 PERFORMING ORGANIZATION NAME AND ADDRESS Arnold Engineering Development Center (DY) Air Force Systems Command Arnold Air Force Station, Tennessee 37389		10. PROGRAM ELEMENT, PROJECT, TASK AREA & WORK UNIT NUMBERS Program Element 65807F
11. CONTROLLING OFFICE NAME AND ADDRESS Arnold Engineering Development Center (DYFS) Arnold Air Force Station, Tennessee 37389		12. REPORT DATE January 1977 13 NUMBER OF PAGES 56
14 MONITORING AGENCY NAME & ADDRESS(if different from Controlling Office)		15. SECURITY CLASS. (of this report) UNCLASSIFIED 15a. DECLASSIFICATION/DOWNGRADING SCHEDULE N/A

16 DISTRIBUTION STATEMENT (of this Report)

Approved for public release; distribution unlimited.

17 DISTRIBUTION STATEMENT (of the abstract entered in Block 20, if different from Report)

18 SUPPLEMENTARY NOTES

Available in DDC

19 KEY WORDS (Continue on reverse side if necessary and identify by block number)

Chapman-Korst	afterbodies
theory	flows
supersonic	boundary layer
nozzle	Mach numbers

20 ABSTRACT (Continue on reverse side if necessary and identify by block number)

A Chapman-Korst-type analysis has been developed for estimating the bulk base flow properties of nozzle-afterbody configurations operating at supersonic speeds. The analysis includes the effects of both initial boundary layers, dissimilar thermodynamic properties of both streams, and a third base bleed gas. The inviscid portions of the jet and external flow are computed by the method of characteristics. The turbulent mixing

DD FORM 1 JAN 73 1473 EDITION OF 1 NOV 65 IS OBSOLETE

UNCLASSIFIED

20. ABSTRACT (Continued)

analysis uses the turbulent kinetic energy method to determine the coefficient in a Prandtl-type eddy viscosity model. The empirical coefficients in the turbulent kinetic energy formulation are those developed for the turbulent mixing of jet flows. A new analytical model of the recompression process has been developed that eliminates the need for an empirical recompression factor to determine the stagnating streamline. The analysis is evaluated by comparing with experimental data for Mach 2.0 flow over a two-dimensional blunt base with hydrogen bleed, a two-dimensional backward-facing step and a hot and a cold rocket nozzle-afterbody configuration. Usually the theoretical base pressure is greater than experimental base pressure, indicating the mixing rate is too small. However, the recompression analysis predicts reasonable values of the recompression factor.

AFSC
Arnold AFS Tenn

PREFACE

The work reported herein was conducted by the Arnold Engineering Development Center (AEDC), Air Force Systems Command (AFSC), under Program Element 65807F. The results were obtained by ARO, Inc. (a subsidiary of The Sverdrup Corporation), contract operator of AEDC, AFSC, Arnold Air Force Station, Tennessee. The work was done under ARO Projects No. R33P-G0A and R33A-02A. The authors of this report were R. C. Bauer and J. H. Fox, ARO, Inc. The manuscript (ARO Control No. ARO-ETF-TR-76-121) was submitted for publication on October 13, 1976.

CONTENTS

Page

1.0 INTRODUCTION 5
2.0 THEORETICAL DEVELOPMENT 8
2.1 Inviscid Flow Fields 11
2.2 Turbulent Mixing Analysis 11
2.3 Recompression Analysis 28
2.4 Solution Conditions 36
3.0 EVALUATION OF THEORY 38
3.1 Davis Experiment 38
3.2 Two-Dimensional Backward-Facing Step Experiments 41
3.3 Rocket-Afterbody Configuration 43
3.4 Reid and Hastings Experiment 45
4.0 CONCLUDING REMARKS 46
REFERENCES 47

ILLUSTRATIONS

Figure

1. Types of Nozzle-Afterbody Flows 6
   a. Attached Flow 6
   b. Boundary-Layer Separation on Afterbody 6
   c. Separation Because of Abrupt Change in Afterbody Geometry 7
2. Idealized Nozzle-Afterbody Flow 9
3. Comparison of Theoretical η_P and ϕ_D with Experiment 12
   a. η_P versus x/δ 12
   b. ϕ_D versus x/δ 13
4. General Mixing Zone 14
5. Variation of Similarity Parameter with Free-Stream Mach No. 25
6. Mixing along Jet Plume Boundary 26
7. Typical Recompression Process 29
8. Illustration of Similarity in the Recompression Pressure Distribution 30

Figure Page

9. Estimated Properties along Stagnating Streamline by Chow (Ref. 17) 31
10. Assumed Recompression Flow Field 32
11. Conditions at Stagnation Point 32
12. Comparison of Theory with Davis Experiment 39
    a. Base Pressure 39
    b. Base Thermodynamic Properties 40
    c. Mixing Similarity Parameter 40
    d. Recompression Factor 41
13. Comparison of Theory with Two-Dimensional Backstep Experiment 42
    a. Initial Boundary-Layer Effect on Base Pressure 42
    b. Mixing Similarity Parameter 42
    c. Recompression Factor 43
14. Application of Theory to a Rocket-Afterbody Configuration 43
    a. Base Pressure 43
    b. Base Thermodynamic Properties 44
    c. Mixing Similarity Parameters 44
    d. Recompression Factors 45
15. Comparison of Theory with Reid and Hastings Experiment 46
    a. Base Pressure 46
    b. Recompression Factors 46

APPENDIX

A. DEFINITION OF INTEGRALS 51

NOMENCLATURE 53

1.0 INTRODUCTION

The afterbody drag of a jet-propelled vehicle is determined by the strong interaction of the engine exhaust with the external stream. Analytical methods to compute afterbody flow fields vary considerably depending on the free-stream Mach number and whether the external flow is attached or separated. For conditions with attached external flow, Fig. 1a, an "effective" body modeling can be useful although there is an unsolved problem of how to represent the jet plume. There are two types of external flow separation: (1) that which occurs when the boundary layer cannot sustain the adverse pressure gradient along the afterbody surface, Fig. 1b, and (2) that caused by an abrupt change in afterbody geometry (Fig. 1c). The second type of flow separation is more amenable to analysis because the separation point is fixed. The latter separated flow is of practical interest for many missile configurations which operate at supersonic Mach numbers. The first type of flow separation is difficult to analyze because of inadequate models for predicting boundary-layer separation phenomena, particularly on aircraft flying at transonic and subsonic Mach numbers. In this report, only flow separation caused by an abrupt change in afterbody geometry will be considered for supersonic external stream Mach numbers. The analysis may then be extended for application to the first type of separation and for all Mach numbers.

The basic analytical approach followed in this report is that developed by Chapman and Korst (Ref. 1). The work of Korst is more closely followed since it deals with turbulent base flow. Other investigators such as Addy, Ref. 2, and Fong, Ref. 3, have applied the Chapman-Korst theory to the identical problem considered herein. All subsequent investigators have recognized that the major discrepancy in the Chapman-Korst theory is the modeling of the recompression process. Addy, Ref. 2, clearly describes how the recompression process has been represented by the various investigators. His description is quoted in the following two paragraphs.

"Since the recompression process is not well understood and does strongly influence the solution to the base-flow problem, the need to improve agreement between predicted and experimental values has resulted in several empirical modifications to this part of the flow model. Nash, Ref. 4, proposed and determined an empirical "reattachment condition" for the supersonic single-stream two-dimensional case which was approximately independent of the supersonic approach Mach number. An approach was adopted by Carrière and Sirieix, Ref. 5, in which they proposed and meticulously determined an empirical law of reattachment, for a negligible initial boundary layer, based on an "angular criterion of turbulent reattachment." Their proposed law of reattachment is shown to correlate well the data for reattachment on a wall of supersonic axisymmetric, two-dimensional, and conical flows. Page, Kessler, and Hill, Ref. 6, offer an alternative

empirical reattachment for two-dimensional supersonic flow based on the "discriminating-streamline" velocity ratio."

"For the axisymmetric two stream base-flow problem under consideration herein, the recompression resulting from the interaction of separated supersonic free-stream nozzle flows apparently cannot be analyzed by a direct carry-over of the empirical reattachment criteria determined in the aforementioned investigations. As a result, Sirieix, Delery, and Mirande, Ref. 7, have presented a more generalized "criterion of turbulent reattachment" which involves geometric as well as flow variables. This criterion is the basis for a limited comparison between predicted and experimental values of the axisymmetric jet-on base pressure ratio. Agreement was improved for the cases presented. More recently, Dixon, Richardson, and Page, Ref. 8, considered this problem under the experimentally supported assumption that the external inviscid flow boundary remains straight after initially turning to adjust to the base pressure. This assumption necessarily results in an axial-pressure gradient from which the internal flow boundary is determined. The corresponding inviscid flow fields thus determined are linked to an approximate axisymmetric mixing component by a recompression criterion based on Goethert's modification of Korst's escape criterion. This approach also improves the agreement between the predicted and experimental results for the cases presented in their paper."

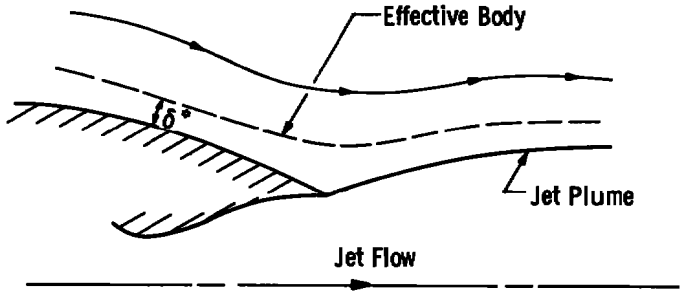

a. Attached flow

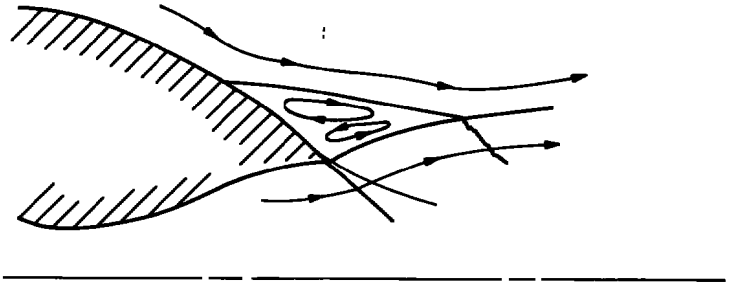

b. Boundary-layer separation on afterbody
Figure 1. Types of nozzle-afterbody flows.

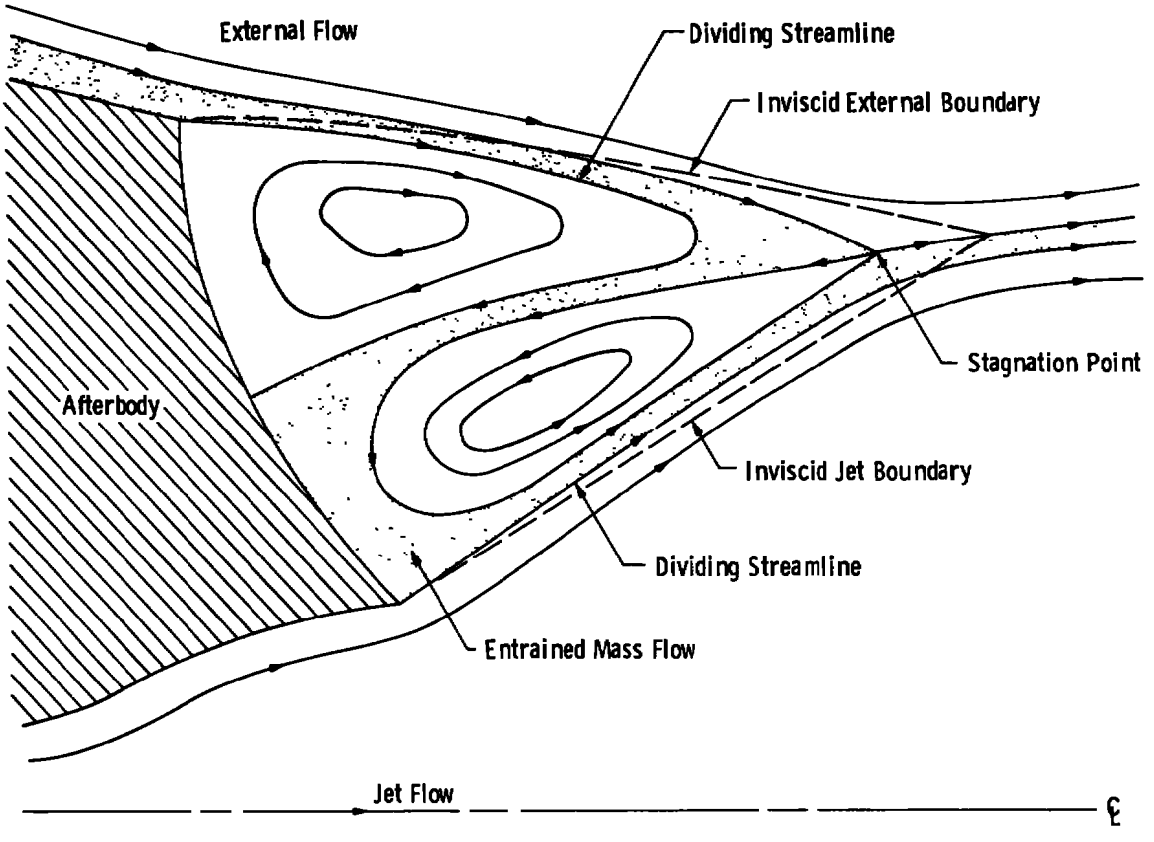

c. Separation because of abrupt change in afterbody geometry
Figure 1. Concluded.

Addy, Ref. 2, presents a relatively simple empirical recompression factor for cylindrical afterbodies that is only a function of the ratio of afterbody radius to jet radius. Unfortunately. Addy's empirical recompression factor had to be modified for conical afterbodies (Ref. 9). Apparently, a universal empirical recompression factor has not yet been developed.

In this report a relatively simple recompression flow model is developed which yields a theoretical value of the recompression factor. The various factors which affect the recompression process are theoretically approximated. The initial boundary layers are included in the turbulent mixing analysis which determines the development with distance of the mixing process. The rate of mixing is based on turbulent kinetic energy concepts and accounts for all differences in thermodynamic properties between the base and the corresponding external stream. Finally, the analysis includes the effects of a third base bleed gas.

2.0 THEORETICAL DEVELOPMENT

The type of afterbody flow analyzed is that in which the flow separates because of an abrupt change in afterbody geometry. A typical streamline pattern associated with this type of afterbody flow is shown in Fig. 1c. In Fig. 1c the streamlines that separate from the afterbody, computed by assuming no mixing, are indicated by dotted lines and are referred to hereinafter as the inviscid jet boundaries. The turbulent mixing process shifts the inviscid streamlines to the solid lines, referred to as the dividing streamlines, which separate the high-speed flow from the entrained flow. The intersection of the two flow fields is referred to as the recompression zone or region. In the recompression zone a slip line is formed and an adverse static pressure gradient exists. A portion of each turbulent mixing zone will not have sufficient mechanical energy (total pressure) to penetrate the adverse static pressure gradient and will be reversed into the separated region. The stagnating streamlines are those streamlines which separate the flow that is reversed into the separated region from the flow that has sufficient mechanical energy to penetrate the adverse static pressure gradient and proceed downstream. For typical afterbody flows, as shown in Fig. 1c, the dividing streamline in the turbulent mixing zone of the external stream does not have sufficient mechanical energy to proceed downstream and is reversed into the separated region, thus forming a vortex. As a result, a portion of the external flow is pumped into the separated region and must be pumped out by the turbulent mixing along the jet boundary. To do this, the dividing streamline in the turbulent mixing zone of the jet flow must have sufficient mechanical energy to proceed downstream. Thus the equilibrium conditions in the separated region are those which make the mass flow pumped in equal to the mass flow pumped out of the separated region. In addition, conservation of energy must simultaneously be established.

The application of the Chapman-Korst base pressure theory to the afterbody flow shown in Fig. 1c requires a simplification of the flow field shown in Fig. 2. The major simplifying assumption is that the double vortex pattern can be replaced by a region of constant fluid properties in which the velocities are negligible. In addition, the base region is highly turbulent and therefore can be assumed to be highly stirred and thus homogeneous. Based on this assumption, the turbulent mixing processes can be estimated by a single-stream, constant pressure mixing analysis. Also, the constant pressure boundary condition can be used to estimate the inviscid portions of the external and jet flows. The complete flow field up to the beginning of the recompression zone can then be obtained by superimposing the mixing zones on the inviscid flow boundaries.

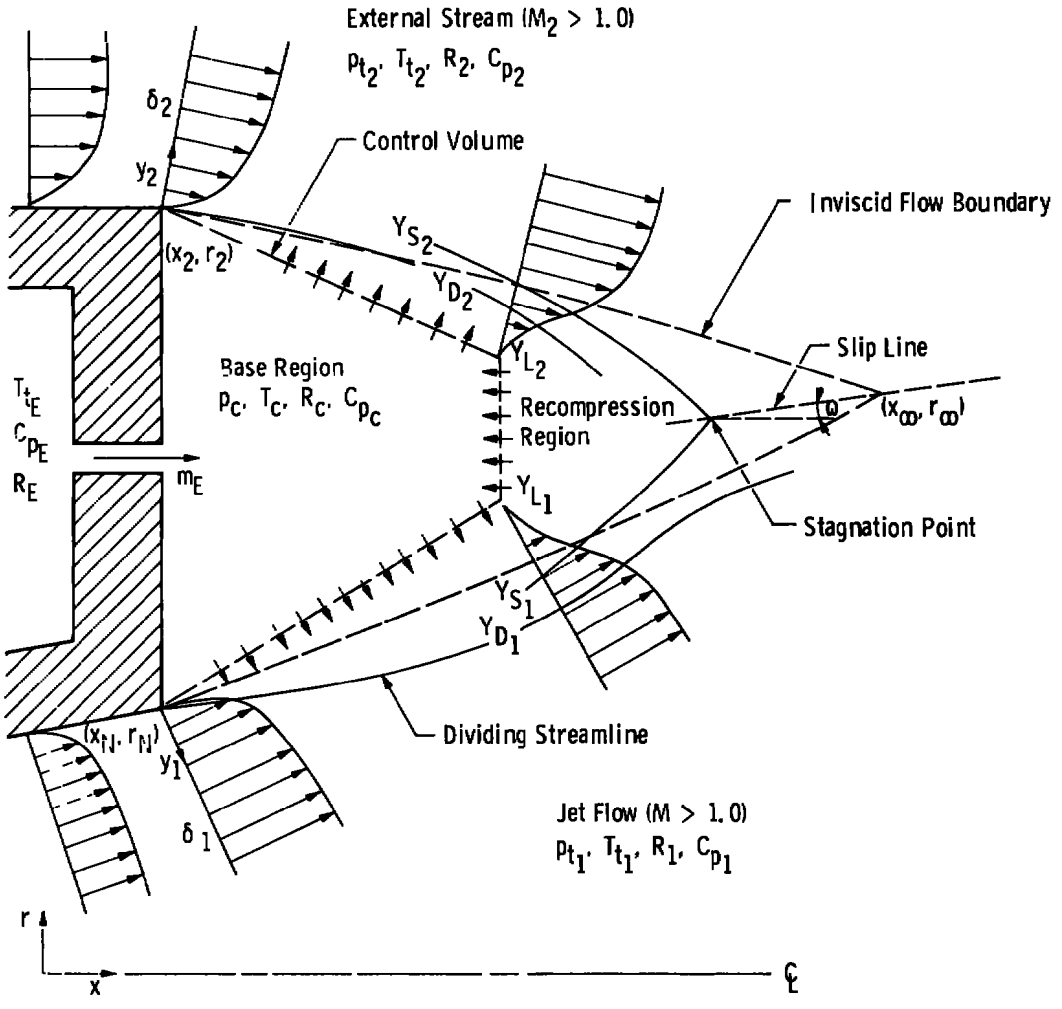

Figure 2. Idealized nozzle-afterbody flow.

In this application of the Chapman-Korst theory the following assumptions are used:

1. The inviscid portions of both the external and the jet flow are supersonic.

2. The base bleed has zero momentum.

3. All the gases obey the Perfect Gas Law.

4. All the gas properties are constant throughout the base region which is defined to be bounded by the afterbody wall, the lower edges of the mixing zones (ϕ = 0.016), and the beginning of the recompression region. In addition, the velocities in this region are negligible.

The basic equations to be solved are those for the conservation of mass and energy for the base region control volume shown in Fig. 2.

The equation for conservation of mass is

$$m_E - 2\pi r_\infty \int_{Y_{L_1}}^{Y_{D_1}} \rho u dY_1 + 2\pi r_\infty \int_{Y_{L_1}}^{Y_{S_1}} \rho u dY_1 - 2\pi r_\infty \int_{Y_{L_2}}^{Y_{D_2}} \rho u dY_2 + 2\pi r_\infty \int_{Y_{L_2}}^{Y_{S_2}} \rho u dY_2 = 0 \tag{1}$$

where the positive sign indicates mass flow into the base region. This equation was written assuming the beginning of the recompression is at the point (x_∞, r_∞) in order to simplify its evaluation. However, this does not introduce any error since Eq. (1) can be written as

$$m_E - 2\pi r_\infty \int_{Y_{D_1}}^{Y_{S_1}} \rho u dY_1 + 2\pi r_\infty \int_{Y_{L_2}}^{Y_{S_2}} \rho u dY_2 = 0 \tag{2}$$

Each integral term in Eq. (2) is the mass flow between the stagnating and dividing streamlines which must be the same for the mixing zones located at the actual beginning of the recompression zone (Fig. 2).

The equation for the conservation of energy in the base region is

$$C_{p_E} T_{t_E} m_E + 2\pi r_\infty \int_{Y_{L_1}}^{Y_{S_1}} C_p T_t \rho u dY_1 + 2\pi r_\infty \int_{Y_{L_2}}^{Y_{S_2}} C_p T_t \rho u dY_2$$

$$- 2\pi r_\infty C_{p_c} T_c \left[\int_{Y_{L_1}}^{Y_{D_1}} \rho u dY_1 + \int_{Y_{L_2}}^{Y_{D_2}} \rho u dY_2 \right] = 0 \tag{3}$$

Again, the mixing zones properties are evaluated at the point (x_∞, r_∞) rather than at the beginning of the recompression. This assumption introduces compensating errors because the first two integral terms overestimate the energy into the base region by the same amount the last two integrals overestimate the energy leaving the base region.

The evaluation of Eqs. (2) and (3) requires complete definition of the inviscid-viscous flow field and the locations of the dividing and stagnating streamlines. In this analysis the inviscid flow fields, the turbulent mixing processes, and the recompression processes are analytically estimated separately and combined by superposition to obtain the

information necessary to evaluate Eqs. (2) and (3). The base region properties are iterated until Eqs. (2) and (3) are satisfied.

2.1 INVISCID FLOW FIELDS

For an assumed base pressure, p_c, the inviscid flow field of both the jet and external stream are computed by the well-known method of characteristics solution of the general potential flow equation for supersonic flow. Both flows are assumed to separate from the physical corners of the afterbody thus neglecting the displacement effect of the initial boundary layers. The major information to be obtained from this calculation is the location of the impingement point (x_∞, r_∞) of the inviscid flow boundaries, the length of each boundary to that point, and the inviscid flow conditions along the high-speed edge of each mixing zone after superposition. The impingement point (x_∞, r_∞) is a point on the slip line that is formed between the two flow fields. The slip-line angle and maximum static pressure are determined by the interaction of the inviscid flows along the high-speed edge of the mixing zones at (x_∞, r_∞). This is an extension of the method developed in Ref. 9 to account for the nonuniformity of the inviscid flow on the recompression process.

2.2 TURBULENT MIXING ANALYSIS

The analysis of each of the two mixing zones is based on the following assumptions:

1. The mixing process is isobaric.

2. The width of the mixing zone is small compared to the radius ($b/r < 0.3$) so that the locations, within the mixing layer, of the dividing streamline and inviscid boundary are the same as for two-dimensional mixing (Ref. 10).

3. For given base and inviscid flow conditions, the eddy viscosity is equal to that for fully developed mixing.

4. The inviscid flow is uniform in the vicinity of the mixing zone and has a velocity equal to its boundary velocity.

5. The Prandtl, Lewis and Schmit numbers are unity.

2.2.1 Velocity Profile

The velocity profile at any station in the mixing region is given by the following equation derived by Korst in Ref. 1.

$$\phi = \frac{1}{2}\left[1 + \operatorname{erf}(\eta - \eta_P)\right] + \frac{\eta_P}{\sqrt{\pi}} \int_0^{1.0} \phi_i \ell^{-\left[\eta - \eta_P\left(\frac{y}{\delta}\right)\right]^2} d\left(\frac{y}{\delta}\right) \tag{4}$$

where

$$\phi_i = \left(\frac{y}{\delta}\right)^{\frac{1}{n}} \text{ (initial boundary layer)} \tag{5}$$

Equation (4) defines a parametric family of velocity profiles in terms of η_P ranging from the initial boundary-layer profile, ϕ_i, for $\eta_P = \infty$, to the fully developed mixing profile $\phi = 1/2(1 + \operatorname{erf} \eta)$ for $\eta_P = 0$. An analytical method has been developed in Ref. 11 for estimating the variation of η_P with (x/δ). However, this method involves a numerical integration along the length of the mixing zone and, as a result, requires significant computer time. A more approximate relationship can be based on assumption (3). For two-dimensional constant pressure mixing the relationship is

$$\eta_P = \frac{\sigma\delta}{x} \tag{6}$$

where σ is the similarity parameter for fully developed mixing. A comparison of Eq. (6) with Chapman's incompressible experimental data (Ref. 12) is presented in Fig. 3a.

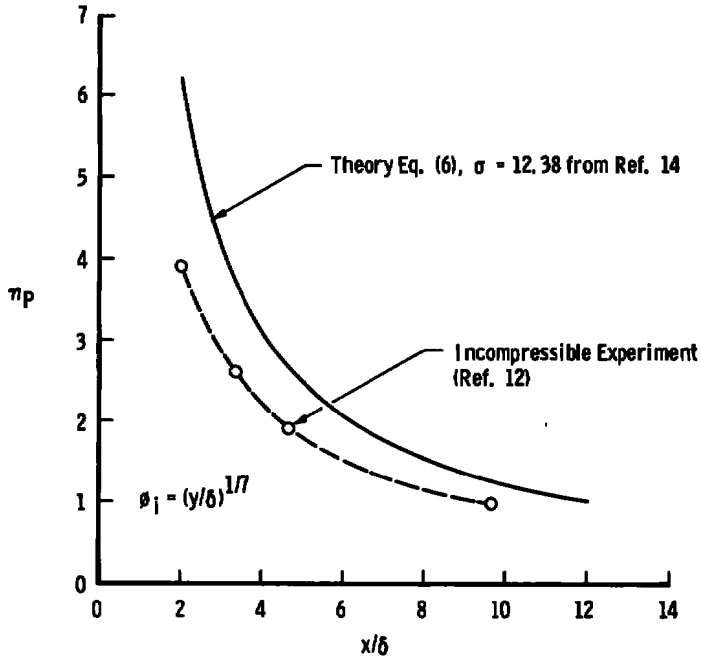

a. η_P vs x/δ

Figure 3. Comparison of theoretical η_P and ϕ_D with experiment.

The theoretical value of η_P is shown always to be greater than experiment which results in an under prediction of the velocity ratio on the dividing streamline as shown in Fig. 3b. Included in Fig. 3b is the "universal" prediction by Alber and Lees (Ref. 13) which overpredicts the dividing streamline velocity ratio by about the same amount the present analysis underpredicts the velocity ratio. Equations (4) and (6) are considered to provide a reasonable representation of the velocity profile development of a turbulent mixing zone strongly influenced by an initial boundary layer.

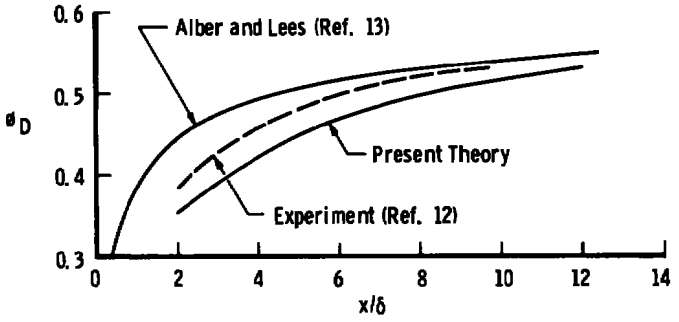

b. ϕ_D vs x/δ

Figure 3. Concluded.

2.2.2 Thermodynamic Composition

The thermodynamic properties of interest in the mixing zone are total temperature, T_t; the gas constant R_g, and the sepcific heat for constant pressure C_p. As a consequence of assumption 5 the thermodynamic properties at any point in the mixing zone are determined by the simple mixture equations for two gases, i.e., the high-speed gas and the base region gas. The equations are

$$\frac{R_g}{R_{g_\infty}} = k + (1 - k)\frac{R_{g_c}}{R_{g_\infty}} \tag{7}$$

and

$$\frac{C_p}{C_{p_\infty}} = k + (1 - k)\frac{C_{p_c}}{C_{p_\infty}} \tag{8}$$

and

$$\frac{T_t}{T_{t_\infty}} = \frac{k + (1 - k)\left(\dfrac{C_{p_c}\,T_c}{C_{p_\infty}\,T_{t_\infty}}\right)}{k + (1 - k)\left(\dfrac{C_{p_c}}{C_{p_\infty}}\right)} \tag{9}$$

where the subscript ∞ indicates the high-speed stream and k is the local mass fraction of the high-speed stream at any point in the mixing zone.

The distribution of k through the mixing zone can be determined by simultaneously solving the conservation of mass and momentum equations. The conservation equations for a typical mixing zone, shown in Fig. 4, are Conservation of Mass Flow:

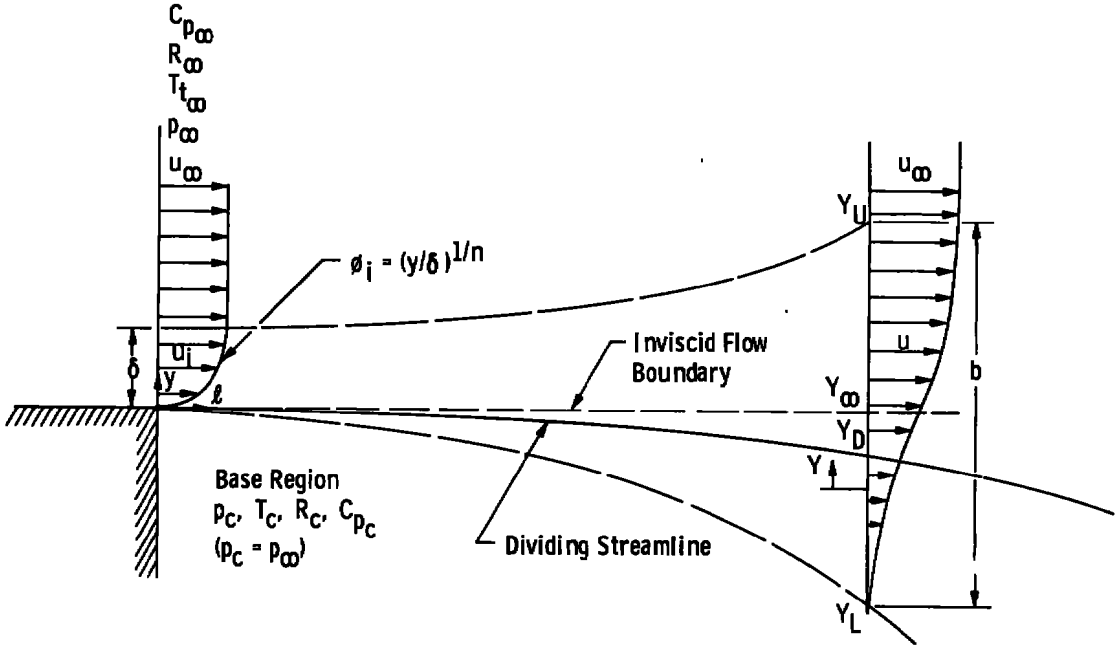

Figure 4. General mixing zone.

$$\int_0^\delta \rho_i u_i dy + \rho_\infty u_\infty [Y_U - Y_\infty - \delta] = \int_{Y_L}^{Y_U} k\rho u dY \tag{10}$$

Conservation of Momentum:

$$\int_0^\delta \rho_i u_i^2 dy + \rho_\infty u_\infty^2 [Y_U - Y_\infty - \delta] = \int_{Y_L}^{Y_U} \rho u^2 dY \tag{11}$$

Combining Eqs. (10) and (11) yields

$$u_\infty \int_0^\delta \rho_i u_i dy - \int_0^\delta \rho_i u_i^2 dy + \int_{Y_L}^{Y_U} \rho u^2 dy = u_\infty \int_{Y_L}^{Y_U} k\rho u dy \tag{12}$$

Since

$$y = Y - Y_\infty$$

$$dy = dY$$

and for $Y \leqslant Y_\infty$

$$\rho_i u_i = 0, \qquad \rho_i u_i^2 = 0$$

for $Y \geqslant Y_\infty + \delta$

$$\rho_i u_i = \rho_\infty u_\infty, \qquad \rho_i u_i^2 = \rho_\infty u_\infty^2$$

Equation (12) can be written as

$$\int_{Y_L}^{Y_U} \left[\rho_i u_i - \frac{\rho_i u_i^2}{u_\infty} + \frac{\rho u^2}{u_\infty} \right] dY = \int_{Y_L}^{Y_U} k \rho u dY \tag{13}$$

Therefore,

$$k = \frac{\rho_i u_i}{\rho u} - \frac{\rho_i u_i^2}{\rho u u_\infty} + \frac{u}{u_\infty} \tag{14}$$

The bounds on $\rho_i u_i$ also apply to Eq. (14), i.e.,

for $Y \leqslant Y_\infty$

$$k = \frac{u}{u_\infty} \tag{15}$$

for $Y_\infty \leqslant Y \leqslant (Y_\infty + \delta)$

$$k = \frac{\rho_i u_i}{\rho u} - \frac{\rho_i u_i^2}{\rho u u_\infty} + \frac{u}{u_\infty} \tag{16}$$

and for $Y > (Y_\infty + \delta)$

$$k = \frac{u}{u_\infty} \tag{17}$$

It should be noted that for zero initial boundary layer $k = u/u_\infty$, which is the well-known Crocco relation for unity Prandtl, Lewis and Schmit numbers.

In terms of the nondimensional mixing variables,

Eq. (11) becomes

$$\eta_\infty = \eta_U - \eta_P \left[\frac{\delta^*}{\delta} + \frac{\theta}{\delta}\right] - \left(1 - C_\infty{}^2\right)\left(I_2\right)_{\eta_U} \tag{18}$$

and Eqs. (15), (16), and (17) become

For $\eta \leq \eta_\infty$

$$k = \phi \tag{19}$$

for $\eta_\infty \leq \eta \leq (\eta_\infty + \eta_P)$

$$k = \phi - \frac{\left(\frac{R_g}{R_{g_\infty}}\right)\left[\frac{T_t}{T_{t_\infty}} - \left(\frac{C_{p_\infty}}{C_p}\right) C_\infty{}^2 \phi^2\right] (\eta - \eta_\infty)^{\frac{1}{n}} \left[\eta_P{}^{\frac{1}{n}} - (\eta - \eta_\infty)^{\frac{1}{n}}\right]}{\phi\left[\eta_P{}^{\frac{2}{n}} - C_\infty{}^2 (\eta - \eta_\infty)^{\frac{2}{n}}\right]} \tag{20}$$

for $\eta \geq (\eta_\infty + \eta_P)$

$$k = \phi \tag{21}$$

Equations (18) through (21) are used to determine η_∞, the location of the inviscid flow boundary in the turbulent mixing zone, which is used to properly superimpose the mixing zone on the inviscid flow field and to establish the mass fraction, k, distribution through the mixing zone.

2.2.3 Location of Dividing Streamline

The location of the dividing streamline in the mixing zone is obtained by applying the conservation of mass condition to the mixing process shown in Fig. 4. The basic equation is

$$\int_0^\delta \rho_i u_i dy + \rho_\infty u_\infty \left[Y_U - Y_\infty - \delta\right] = \int_{Y_D}^{Y_U} \rho u dy \tag{22}$$

Since Eq. (22) involves Y_∞, it is necessary to combine Eq. (22) with the conservation of momentum equation [Eq. (11)] to yield

$$u_\infty \int_0^\delta \rho_i u_i dy - \int_0^\delta \rho_i u_i{}^2 dy + \int_{Y_L}^{Y_U} \rho u^2 dY = u_\infty \int_{Y_D}^{Y_U} \rho u dY \tag{23}$$

By definition

$$\rho_\infty u_\infty \, [\delta - \delta^*] = \int_0^\delta \rho_i u_i dy \tag{24}$$

and

$$\rho_\infty u_\infty^2 [\delta - \delta^* - \theta] = \int_0^\delta \rho_i u_i^2 dy \tag{25}$$

Thus, Eq. (23) becomes

$$\rho_\infty u_\infty^2 \theta + \int_{Y_L}^{Y_U} \rho u^2 dY = u_\infty \int_{Y_L}^{Y_U} \rho u dY - u_\infty \int_{Y_L}^{Y_D} \rho u dY \tag{26}$$

In nondimensional form Eq. (26) is

$$(I_1)_{\eta_D} = (I_1)_{\eta_U} - (I_2)_{\eta_U} - \frac{\eta_P}{(1 - C_\infty^2)} \left(\frac{\theta}{\delta}\right) \tag{27}$$

and Eqs. (24) and (25) become

$$\frac{\delta^*}{\delta} = 1 - (1 - C_\infty^2) \int_0^{1.0} \frac{\phi_i}{1 - C_\infty^2 \phi_i^2} \, d\left(\frac{y}{\delta}\right) \tag{28}$$

and

$$\frac{\theta}{\delta} = (1 - C_\infty^2) \int_0^{1.0} \frac{\phi_i (1 - \phi_i)}{1 - C_\infty^2 \phi_i^2} \, d\left(\frac{y}{\delta}\right) \tag{29}$$

2.2.4 The Similarity Parameter, σ

In the previous section the mixing velocity profile is defined in terms of the position parameter, η_P. However, to determine η_P, the similarity parameter, σ, for planar, fully developed, constant pressure turbulent mixing is determined by applying the turbulent kinetic energy (TKE) method to the mixing zone shown in Fig. 4 for no initial boundary layer. The planar value is then corrected for axisymmetric effects. The basic equation is

$$\frac{\rho_\infty u_\infty^3}{2} (Y_U - Y_\infty) - \frac{1}{2} \int_{Y_L}^{Y_U} \rho u^3 dY = \int_{Y_L}^{Y_U} \rho u K dY + \int_{Y_L}^{Y_U} X D dY \tag{30}$$

where

$$K = \frac{1}{2}\left[\overline{(u')^2} + \overline{(u')^2} + \overline{(u')^2}\right] \tag{31}$$

and D = dissipation per unit volume

Equation (30) states that the loss in mean flow kinetic energy (production of TKE) equals the convection of TKE at station x plus the total dissipation in the region between x = 0 and x. For isotropic turbulence the dissipation is

$$D = \frac{a_2 \rho K^{3/2}}{b} \tag{32}$$

By definition

$$b = \eta_b \left(\frac{\ell}{\sigma}\right) \tag{33}$$

$$\therefore D = \frac{a_2 \rho K^{3/2}}{\eta_b}\left(\frac{\sigma}{\ell}\right) \tag{34}$$

Substituting into Eq. (30) yields

$$\frac{\rho_\infty u_\infty^3}{2}(\eta_U - \eta_\infty) - \frac{1}{2}\int_{\eta_L}^{\eta_U} \rho u^3 d\eta = \int_{\eta_L}^{\eta_U} \rho u K d\eta + \int_{\eta_L}^{\eta_U}\left(\frac{a_2\sigma}{\eta_b}\right)\rho K^{3/2} d\eta \tag{35}$$

Dividing by $\rho_\infty u_\infty^3$

$$\frac{(\eta_U - \eta_\infty)}{2} - \frac{1}{2}\int_{\eta_L}^{\eta_U}\left(\frac{\rho}{\rho_\infty}\right)\phi^3 d\eta = \int_{\eta_L}^{\eta_U}\left(\frac{\rho}{\rho_\infty}\right)\phi\left(\frac{K}{u_\infty^2}\right) d\eta + \int_{\eta_L}^{\eta_U}\left(\frac{a_2\sigma}{\eta_b}\right)\left(\frac{\rho}{\rho_\infty}\right)\left(\frac{K}{u_\infty^2}\right)^{3/2} d\eta \tag{36}$$

For a perfect gas

$$\rho = \frac{p_c}{R_g T} = \frac{p_c}{R_g T_t\left(\frac{T}{T_t}\right)} = \frac{p_c}{R_g T_t(1 - C^2)}$$

and

$$\rho_\infty = \frac{p_c}{R_{g_\infty} T_\infty} = \frac{p_c}{R_{g_\infty} T_{t_\infty}(1 - C_\infty^2)}$$

$$\therefore \frac{\rho}{\rho_\infty} = \left(\frac{R_{g_\infty}}{R_g}\right)\left(\frac{T_{t_\infty}}{T_t}\right)\frac{(1 - C_\infty{}^2)}{(1 - C^2)} \tag{37}$$

By definition

$$C^2 = \frac{u^2}{2\, C_p\, T_t}$$

and

$$C_\infty{}^2 = \frac{u_\infty{}^2}{2\, C_{p_\infty}\, T_{t_\infty}}$$

$$\therefore \frac{C^2}{C_\infty{}^2} = \left(\frac{C_{p_\infty}}{C_p}\right)\left(\frac{T_{t_\infty}}{T_t}\right)\phi^2 \tag{38}$$

or

$$\frac{\rho}{\rho_\infty} = \frac{(1 - C_\infty{}^2)}{\dfrac{R_g}{R_{g_\infty}}\left[\dfrac{T_t}{T_{t_\infty}} - \left(\dfrac{C_{p_\infty}}{C_p}\right) C_\infty{}^2\, \phi^2\right]} \tag{39}$$

Substituting Eq. (39) into Eq. (36) yields

$$\frac{(\eta_U - \eta_\infty)}{2} - \frac{(1 - C_\infty{}^2)}{2}(I_3)_{\eta_U} = (1 - C_\infty{}^2)\int_{\eta_L}^{\eta_U} \frac{\dfrac{K}{u_\infty{}^2}\,\phi\, d\eta}{\dfrac{R_g}{R_{g_\infty}}\left[\dfrac{T_t}{T_{t_\infty}} - \left(\dfrac{C_{p_\infty}}{C_p}\right) C_\infty{}^2\, \phi^2\right]}$$

$$+ (1 - C_\infty{}^2)\int_{\eta_L}^{\eta_U} \frac{\left(\dfrac{a_2\sigma}{\eta_b}\right)\left(\dfrac{K}{u_\infty{}^2}\right)^{3/2} d\eta}{\dfrac{R_g}{R_{g_\infty}}\left[\dfrac{T_t}{T_{t_\infty}} - \left(\dfrac{C_{p_\infty}}{C_p}\right) C_\infty{}^2\, \phi^2\right]} \tag{40}$$

Substituting Eq. (18) for no boundary layer into Eq. (40) yields

$$\frac{1}{2}\left[(I_2)_{\eta_U} - (I_3)_{\eta_U}\right] = \int_{\eta_L}^{\eta_U} \frac{\left(\frac{K}{u_\infty^2}\right)\phi \, d\eta}{\frac{R_g}{R_{g_\infty}}\left[\frac{T_t}{T_{t_\infty}} - \left(\frac{C_{p_\infty}}{C_p}\right) C_\infty^2 \phi^2\right]} + \int_{\eta_L}^{\eta_U} \frac{\left(\frac{a_2\sigma}{\eta_b}\right)\left(\frac{K}{u_\infty^2}\right)^{3/2} d\eta}{\frac{R_g}{R_{g_\infty}}\left[\frac{T_t}{T_{t_\infty}} - \left(\frac{C_{p_\infty}}{C_p}\right) C_\infty^2 \phi^2\right]} \tag{41}$$

Equation (41) is the TKE equation which is solved by using the empirical information for a_2 and K developed by Peters (Ref. 14).

Let

$$\bar{K} = \frac{K}{K_m} \tag{42}$$

where

$$K_m = K \text{ at } \phi = \frac{1}{2}$$

Substituting Eq. (42) into Eq. (41) yields

$$\frac{1}{2}\left[(I_2)_{\eta_U} - (I_3)_{\eta_U}\right] = \frac{K_m}{u_\infty^2} \int_{\eta_L}^{\eta_U} \frac{\bar{K}\phi \, d\eta}{\frac{R_g}{R_{g_\infty}}\left[\frac{T_t}{T_{t_\infty}} - \left(\frac{C_{p_\infty}}{C_p}\right) C_\infty^2 \phi^2\right]}$$

$$+ \left(\frac{K_m}{u_\infty^2}\right)^{3/2} \int_{\eta_L}^{\eta_U} \frac{\left(\frac{a_2\sigma}{\eta_b}\right)\bar{K}^{3/2} \, d\eta}{\frac{R_g}{R_{g_\infty}} \frac{T_t}{T_{t_\infty}} - \left(\frac{C_{p_\infty}}{C_p}\right) C_\infty^2 \phi^2} \tag{43}$$

Assume:

$$\tau_m = a_1 \rho_m K_m \text{ (shear stress at } \phi = \tfrac{1}{2}\text{)}$$

or

$$\frac{\tau_m}{\rho_\infty u_\infty^2} = a_1 \left(\frac{\rho_m}{\rho_\infty}\right)\left(\frac{K_m}{u_\infty^2}\right)$$

$$\therefore \frac{K_m}{u_\infty^2} = \frac{1}{a_1}\left(\frac{\rho_\infty}{\rho_m}\right)\left(\frac{\tau_m}{\rho_\infty u_\infty^2}\right) \tag{44}$$

also assume a_1, a_2, σ and η_b are independent of η.

Therefore, Eq. (43) becomes as follows

$$\frac{1}{2}\left[(I_2)_{\eta_U} - (I_3)_{\eta_U}\right] = \frac{1}{a_1}\left(\frac{\rho_\infty}{\rho_m}\right)\left(\frac{\tau_m}{\rho_\infty u_\infty^2}\right)\int_{\eta_L}^{\eta_U} \frac{\bar{K}\,\phi\, d\eta}{\frac{R_g}{R_{g_\infty}}\left[\frac{T_t}{T_{t_\infty}} - \left(\frac{C_{p_\infty}}{C_p}\right) C_\infty^2 \phi^2\right]}$$

$$+ \frac{1}{a_1^{3/2}}\left(\frac{\rho_\infty}{\rho_m}\right)^{3/2}\left(\frac{\tau_m}{\rho_\infty u_\infty^2}\right)\left(\frac{a_2\sigma}{\eta_b}\right)\int_{\eta_L}^{\eta_U} \frac{\bar{K}^{3/2}\, d\eta}{\frac{R_g}{R_{g_\infty}}\left[\frac{T_t}{T_{t_\infty}} - \left(\frac{C_{p_\infty}}{C_p}\right) C_\infty^2 \phi^2\right]} \tag{45}$$

The shear stress distribution in the mixing zone can be determined by applying the Conservation of Momentum Equation as in Ref. 1.

The general equation is

$$\frac{\tau}{\rho_\infty u_\infty^2} = \frac{(1 - C_\infty^2)}{\sigma}\left[(I_2)_\eta - \phi\left[(I_1)_\eta - (I_1)_{\eta_D}\right]\right]$$

Therefore, at $\phi = 1/2$ and $\eta = 0$ for fully developed mixing,

$$\frac{\tau_m}{\rho_\infty u_\infty^2} = \frac{(1 - C_\infty^2)}{\sigma}\left[(I_2)_0 - \frac{1}{2}\left[(I_1)_0 - (I_1)_{\eta_D}\right]\right] \tag{46}$$

Substituting Eq. (46) into Eq. (45) yields

$$\sigma\left[(I_2)_{\eta_U} - (I_3)_{\eta_U}\right] - \left[\frac{2a_2 (I_5)_{\eta_U}}{a_1^{3/2}\,\eta_b}\right]\sigma^{1/2} - \left(\frac{2}{a_1}\right)(I_4)_{\eta_U} = 0 \tag{47}$$

For the present set of variables, Peters' distribution of $\bar{K}$ in the mixing zone is

For $\quad \eta < -\left(\frac{\eta_b}{2}\right) \qquad \bar{K} = 0$

For $-\left(\frac{\eta_b}{2}\right) \leq \eta \leq 0.1\left(\frac{\eta_b}{2}\right)$

$$\bar{K} = 0.51\left[1 - \cos\left[3.4268 - 5.7114\left(\frac{\eta}{\eta_b}\right)\right]\right] \tag{48}$$

for $0.1\left(\frac{\eta_b}{2}\right) \leq \eta \leq \frac{\eta_b}{2}$

$$\bar{K} = 0.51\left[1 - \cos\left[3.4906 - 6.9813\left(\frac{\eta}{\eta_b}\right)\right]\right] \tag{49}$$

$$\bar{K} = 0 \quad \text{for} \quad \eta > \frac{\eta_b}{2}$$

The two remaining unknowns in Eq. (47) are a_1 and a_2. Peters assumes a_1 has a universal value of 0.3, and a_2 is a function of the turbulent Reynolds number defined as

$$R_T = \frac{u_\infty b}{\epsilon_m} \tag{50}$$

Since

$$\tau_m = \rho_m \epsilon_m \left.\frac{\partial u}{\partial Y}\right|_m \tag{51}$$

ϵ_m in Eq. (50) can be eliminated to yield

$$R_T = \frac{b}{\left(\frac{\tau_m}{\rho_\infty u_\infty^2}\right)} \left(\frac{\rho_m}{\rho_\infty}\right) \left.\frac{\partial \phi}{\partial Y}\right|_m \tag{52}$$

Substituting Eqs. (33) and (46) into Eq. (52) yields

$$R_T = \frac{\sigma \eta_b \left(\frac{\rho_m}{\rho_\infty}\right) \left.\frac{\partial \phi}{\partial \eta}\right|_m}{(1 - C_\infty^2)\left[(I_2)_0 - \frac{1}{2}\left[(I_1)_0 - (I_1)_{\eta_D}\right]\right]} \tag{53}$$

For fully developed turbulent mixing the velocity profile assumed by Peters is

$$\phi = \frac{1}{2}\left[1 + \cos\left[\frac{\pi}{2} - \pi\left(\frac{\eta}{\eta_b}\right)\right]\right] \tag{54}$$

$$\therefore \left.\frac{\partial\phi}{\partial\eta}\right|_m = \frac{\pi}{2\eta_b} \quad \left(\text{for } \phi = \frac{1}{2}\right) \tag{55}$$

From Eqs. (39), (7), (8), and (9)

$$\frac{\rho_m}{\rho_\infty} = \frac{\left(1 + \frac{C_{p_c}}{C_{p_\infty}}\right)(1 - C_\infty{}^2)}{\left(1 + \frac{R_{g_c}}{R_{g_\infty}}\right)\left[\frac{1}{2}\left(1 + \frac{C_{p_c} T_c}{C_{p_\infty} T_{t_\infty}}\right) - \frac{C_\infty{}^2}{4}\right]} \tag{56}$$

Substituting Eqs. (55) and (56) into Eq. (53) yields

$$R_T = \frac{2\pi\sigma\left(1 - \frac{C_{p_c}}{C_{p_\infty}}\right)}{\left(1 + \frac{R_{g_c}}{R_{g_\infty}}\right)\left[2\left(1 + \frac{C_{p_c} T_c}{C_{p_\infty} T_{t_\infty}}\right) - C_\infty{}^2\right]\left[(I_2)_0 - \frac{1}{2}\left[(I_1)_0 - (I_1)_{\eta_D}\right]\right]} \tag{57}$$

Peters empirically defines a_2 as

For $0 \leq R_T \leq 70$

$$a_2 = \frac{0.99 + 0.01\, R_T}{C} \tag{58}$$

For $70 \leq R_T \leq 145.223$

$$a_2 = \frac{1.69}{C} \tag{59}$$

For $R_T > 145.223$

$$a_2 = \frac{3.3 - 5.19 e^{-0.00806 R_T}}{C} \tag{60}$$

where c is empirically defined as

For $\dfrac{R_{g_\infty} T_{t_\infty}}{R_{g_c} T_c}(1 - C_\infty^2) > 1.0$

$$C = 0.984 + 0.016 \left(\frac{R_{g_\infty} T_{t_\infty}}{R_{g_c} T_c}\right)(1 - C_\infty^2) \tag{61}$$

For $\dfrac{R_{g_\infty} T_{t_\infty}}{R_{g_c} T_c}(1 - C_\infty^2) \leq 1.0$

$$C = 0.95 + 0.05 \left(\frac{R_{g_c} T_c}{R_{g_\infty} T_{t_\infty}}\right) \tag{62}$$

The limits η_L and η_U on the integrals I_1, I_2, I_3, and I_4 are taken to be -3.0 and +3.0, respectively, to obtain an accuracy equal to that obtained by Korst (Ref. 1). These limits correspond to velocity ratios of 0.00001105 and 0.99998895, respectively, for the fully developed mixing velocity given by $\phi = 1/2(1 + \text{erf}\,\eta)$. Peters used the following equation to determine σ:

$$\sigma = \frac{3.12}{\frac{db}{dx}} \tag{63}$$

From Eq. (33)

$$\frac{db}{dx} = \frac{\eta_b}{\sigma} \tag{64}$$

Substituting Eq. (64) into Eq. (63) yields

$$\eta_b = 3.12 \tag{65}$$

Based on these values for η_L, η_U, and η_b the variation of σ with Mach number computed by this method is compared with that by Peters in Fig. 4. As shown, σ determined by the present method is about ten percent less than that determined by Peters. This is believed to be caused by the use of an error function velocity profile rather than the cosine profile used by Peters. Included in Fig. 5 is the estimated σ variation with Mach number based on the well-known Donaldson and Gray correlation of eddy viscosity, Ref. 21. The TKE method was used in the present afterbody analysis because the empirical constants are believed to be more general than those based on the eddy viscosity concept.

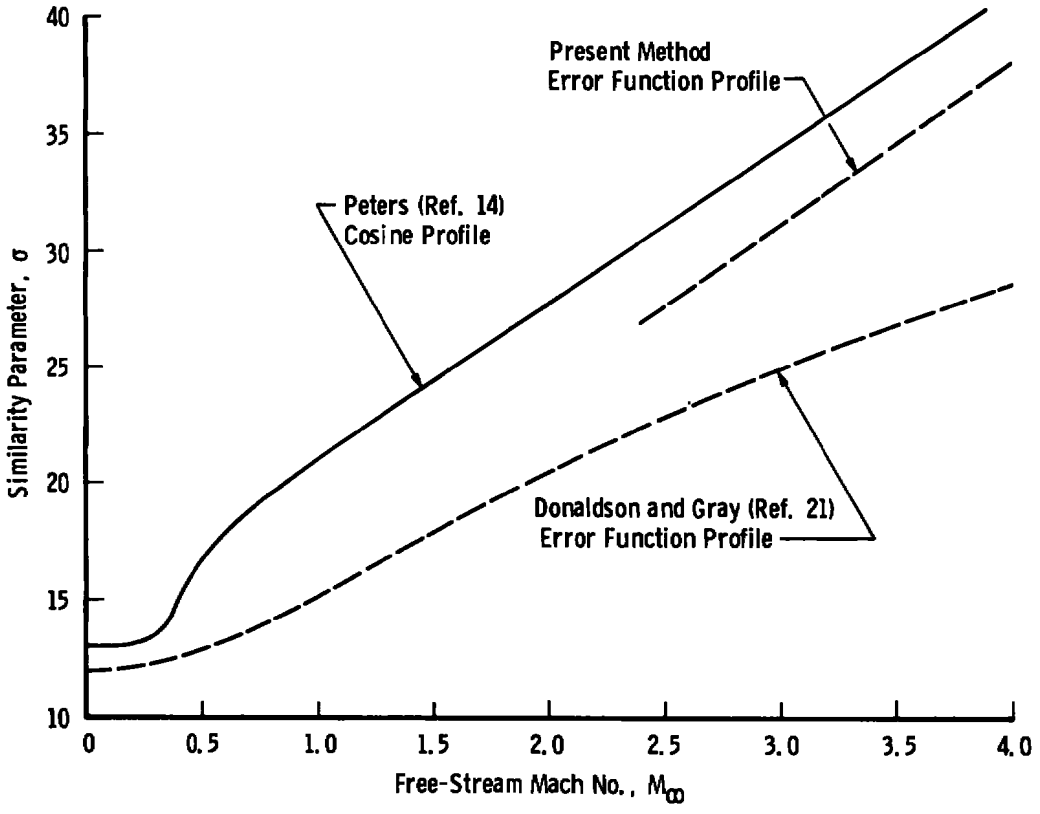

Figure 5. Variation of similarity parameter with free-stream Mach No.

2.2.5 Axisymmetric Effect on σ

Although the assumption that the width of the mixing zone is small compared to the radius does not eliminate an axisymmetric effect on the similarity parameter, σ, it does allow a simple correction to be applied. The correction factor is derived for the mixing along the jet plume boundary. The jet plume boundary, indicated in Fig. 6, is assumed to be a conical surface. The condition applied is that the momentum of the entrained mass flow equals the total shear force along the dividing streamline. The basic equation is

$$\frac{\tau x \, 2\pi(r_N + r)}{2 \cos\beta} = \int_{Y_L}^{Y_D} \rho u^2 \frac{2\pi}{2} \left[r + \left[r - (Y - Y_\infty) \cos\beta\right]\right] dY \tag{66}$$

Let

$$\eta = \frac{\sigma_A Y \cos\beta}{x}; \quad dY = \left(\frac{x}{\sigma_A \cos\beta}\right) d\eta; \quad Y = \left(\frac{x}{\sigma_A \cos\beta}\right) \eta$$

where

σ_A = axisymmetric σ

$$\therefore \frac{\tau x(r_N + r)}{\cos\beta} = \frac{x}{\sigma_A \cos\beta} \int_{\eta_L}^{\eta_D} \rho u^2 \left[2r - \left(\frac{x}{\sigma_A}\right) (\eta - \eta_\infty) \right] d\eta \tag{67}$$

or

$$\tau \sigma_A (r_N + r) = 2r \int_{\eta_L}^{\eta_D} \rho u^2 d\eta - \left(\frac{x}{\sigma_A}\right) \int_{\eta_L}^{\eta_D} \rho u^2 (\eta - \eta_\infty) d\eta \tag{68}$$

Since by definition

$$\eta_b = \frac{\sigma_A b \cos\beta}{x}$$

Eq. (68) can be written

$$\frac{\tau\sigma_A}{2} \left(\frac{r_N + r}{r}\right) = \int_{\eta_L}^{\eta_D} \rho u^2 d\eta - \left(\frac{b}{r}\right) \left(\frac{\cos\beta}{2\eta_b}\right) \int_{\eta_L}^{\eta_D} \rho u^2 (\eta - \eta_\infty) d\eta \tag{69}$$

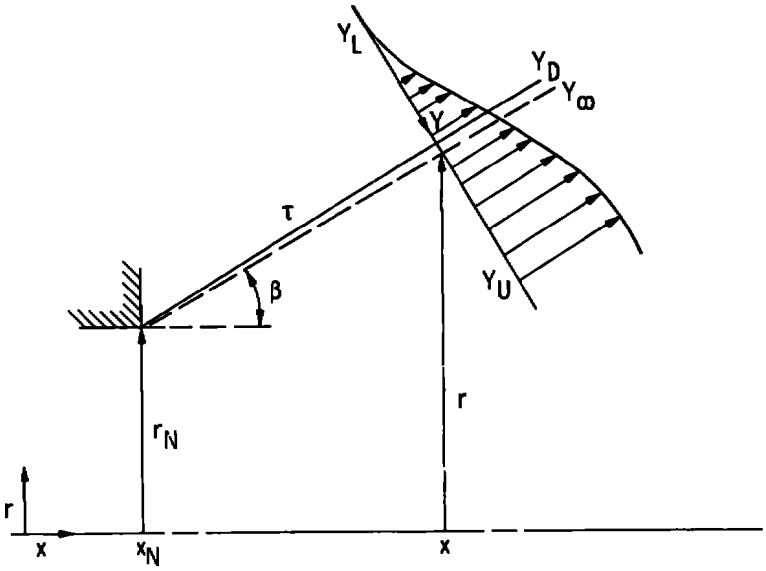

Figure 6. Mixing along jet plume boundary.

By assumption 2

For $b/r \leqslant 0.3$

$$\left(\frac{b}{r}\right)\left(\frac{\cos\beta}{2\eta_b}\right)\int_{\eta_L}^{\eta_D} \rho u^2((\eta - \eta_\infty)d\eta \ll \int_{\eta_L}^{\eta_D} \rho u^2 d\eta \tag{70}$$

The condition expressed by Eq. (70) is numerically verified by the following example:

For $\frac{b}{r} = 0.3$

$$M_\infty = 3.0$$

From Ref. 10

$$\eta_D = 0.3115$$

$$\eta_\infty = 0.7388$$

$$\int_{-3.0}^{\eta_D} \rho u^2 d\eta = \frac{0.23}{\rho_\infty u_\infty^2}$$

$$\int_{-3.0}^{\eta_D} \rho u^2 \eta d\eta = 0$$

and also assume

$$\beta = 0°$$

$$\eta_b = 3.12$$

Substituting into relation (70) gives

$$-0.0335 \ll 1.0$$

thus verifying relation (70) for this set of conditions.

Therefore, Eq. (69) can be written

$$\frac{\pi\sigma_A}{2}\left(\frac{r_N + r}{r}\right) = \int_{\eta_L}^{\eta_D} \rho u^2 d\eta \tag{71}$$

If the mixing were two-dimensional the basic equation would be

$$\frac{\tau x}{\cos \beta} = \int_{Y_L}^{Y_D} \rho u^2 dY \tag{72}$$

and in the transformed plane

$$\tau\sigma = \int_{\eta_L}^{\eta_D} \rho u^2 d\eta \tag{73}$$

Substituting Eq. (73) into Eq. (71)

$$\frac{\tau\sigma_A}{2}\left(\frac{r_N + r}{r}\right) = \tau\sigma$$

Letting $R = \frac{r}{r_N}$ yields

$$\sigma_A = \left(\frac{2R}{1 + R}\right)\sigma \tag{74}$$

In a similar manner the correction factor for the external stream mixing can be shown to be

$$\sigma_A = \left(\frac{2R}{R_2 + R}\right)\sigma \tag{75}$$

Equation (74) shows that σ for mixing along an expanding plume is always greater than that for two-dimensional mixing, whereas for a converging plume Eq. (75) shows that σ is always less than the two-dimensional value.

2.3 RECOMPRESSION ANALYSIS

The most important aspect of the recompression process that must be analytically modeled is that the magnitude of the pressure at the stagnation point is between the base pressure, p_c, and the maximum recompression pressure, p_3, is illustrated in Fig. 7 for the case of rearward-facing step. Originally, Chapman and Korst assumed the stagnation pressure to be the peak pressure, p_3, but this was disproved by Nash (Ref. 4). Recently two observations have been published concerning the recompression process that suggests the phenomena can be realistically represented by a relatively simple analytical model. The two observations are:

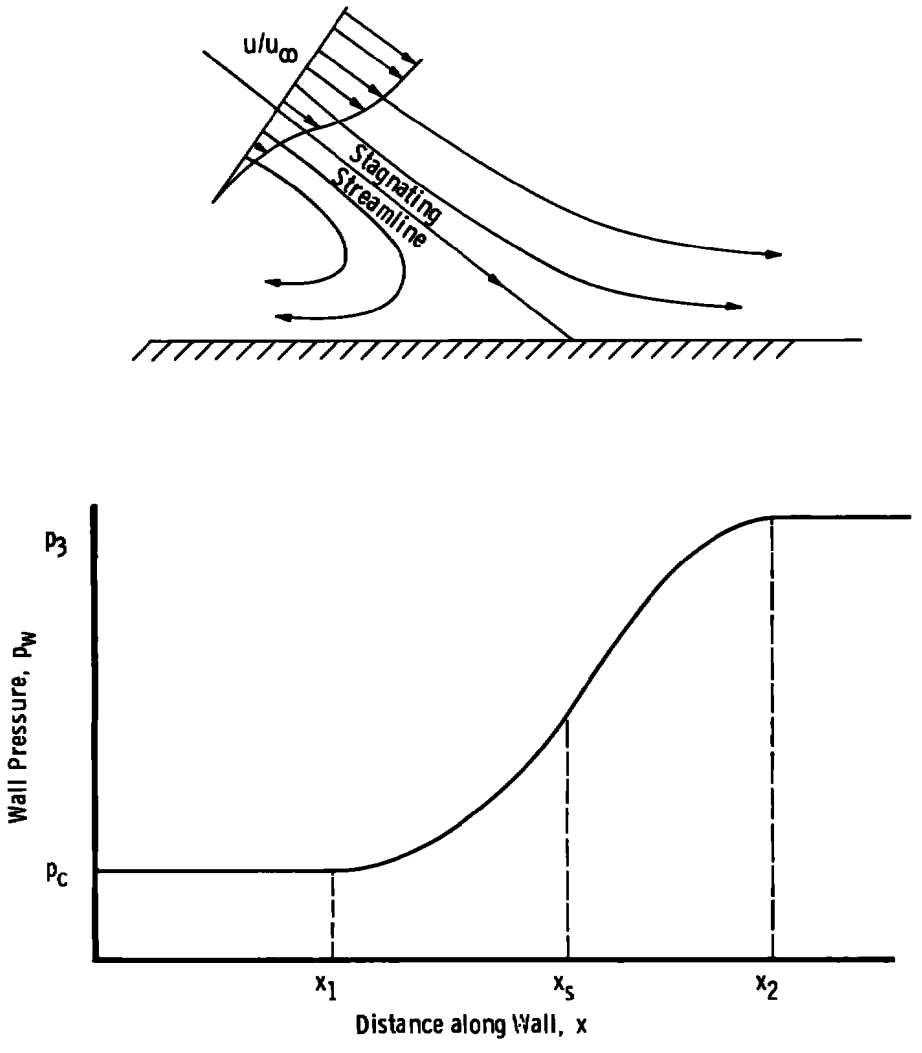

Figure 7. Typical recompression process.

1. Narayanan, et al., Ref. 15, experimentally show that for incompressible planar flow the pressure distribution in the recompression zone has "almost perfect similarity" using the similarity variables $(p - p_c)/(p_3 - p_c)$ and $(x - x^*)/h$. In the present analysis it is convenient to use the similarity variable $(x - x_1)/(x_2 - x_1)$ which is related to $(x - x^*)/h$ by

$$\frac{x - x_1}{x_2 - x_1} = \frac{\left(\frac{x - x^*}{h}\right) - \left(\frac{x_1 - x^*}{h}\right)}{\left(\frac{x_2 - x^*}{h}\right) - \left(\frac{x_1 - x^*}{h}\right)} \tag{76}$$

From the experiments presented in Ref. 15

$$\frac{x_1 - x^*}{h} = -2; \quad \frac{x_2 - x^*}{h} = 2$$

$$\frac{x - x_1}{x_2 - x_1} = \frac{1}{4}\left[\left(\frac{x - x^*}{h}\right) + 2\right]$$

Fig. 8 compares the experimental data of Ref. 15 with the assumed relation between the similarity variables.

$$\therefore \quad \frac{p - p_c}{p_3 - p_c} = \sin^2 \frac{\pi}{2}\left[\frac{x - x_1}{x_2 - x_1}\right] \tag{77}$$

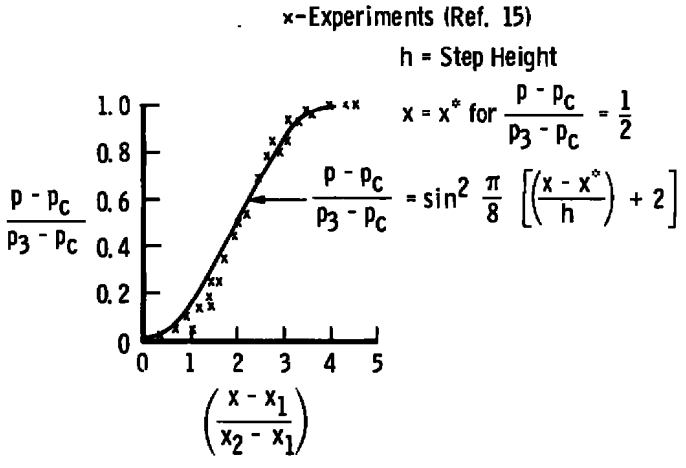

Figure 8. Illustration of similarity in the recompression pressure distribution.

Since values of the similarity variables $(p - p_c)/(p_3 - p_c)$ and $(x - x_1)/(x_2 - x_1)$ are always between 0 and 1.0 it is reasonable to assume Eq. (77) also applies for planar supersonic flow. This is verified by the theoretical and experimental pressure distributions presented by Alber and Lees, Ref. 13, and by experimental results of Viswanath and Narasimha, Ref. 16.

2. Chow's analysis of the recompression process for flow over a backward-facing step presented in Ref. 17 shows that the total pressure on the stagnating streamline continues to increase at about the same rate all the way to the stagnation point on the wall. This result is presented in Fig. 9. The same phenomena was reported by O'Leary and Mueller in Ref. 18 from a numerical solution of the Navier-Stokes equation for incompressible laminar flow over a backward-facing step. Based on these results it is assumed that the

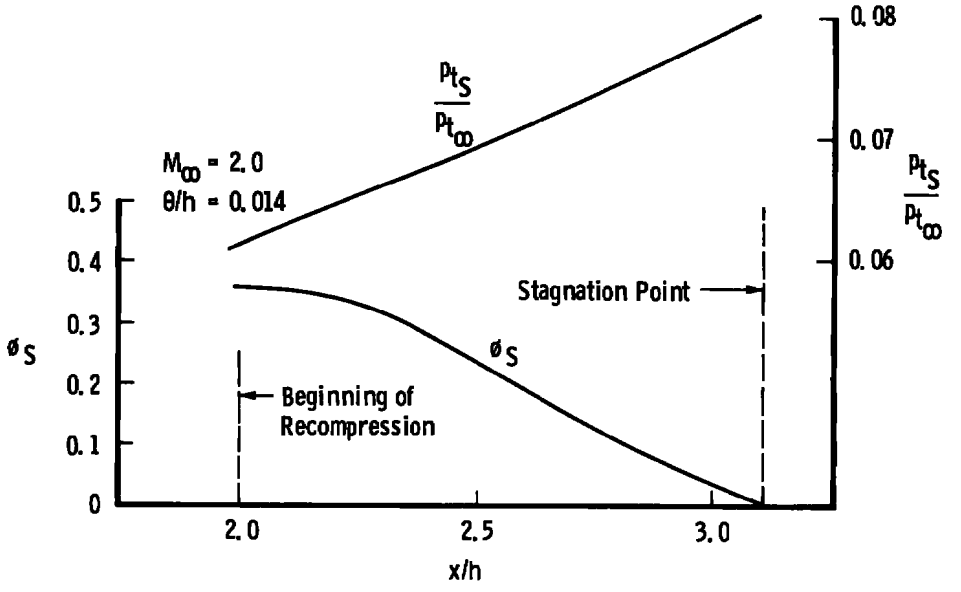

Figure 9. Estimated properties along stagnating streamline by Chow (Ref. 17).

adverse pressure gradient along the stagnating streamline in the recompression zone does not significantly alter the gradient of total pressure compared to a constant pressure shear layer. Therefore, the total-pressure development through the recompression zone to the stagnation point can be estimated by the constant pressure mixing analysis neglecting the adverse pressure gradient.

2.3.1 Analytical Model

The recompression flow field is modeled in a manner similar to that presented in Ref. 9. The assumed flow field is presented in Fig. 10. The mixing is superimposed on the inviscid flow boundary in its proper position as determined by conservation of momentum, Eq. (18). The reverse flow is assumed to turn symmetrically about a line emanating from the stagnation point at half the angle of the stagnating streamline. The intersection of the symmetry line with the lower edge of the mixing zone (defined to be where $\phi = 0.016$) determines the beginning of the recompression process, x_1. The end of the recompression region, x_2, is defined to be the location of the maximum slip line static pressure, p_3. Since an isobaric turbulent mixing process simply redistributes the momentum of the inviscid flow, the total-pressure force between x_1 and x_2 must equal that for inviscid flow. Applying this condition for uniform inviscid flow and the slip line pressure distribution given by Eq. (77) yields the following equation for x_2

$$x_2 = 2x_\infty - x_1 \tag{78}$$

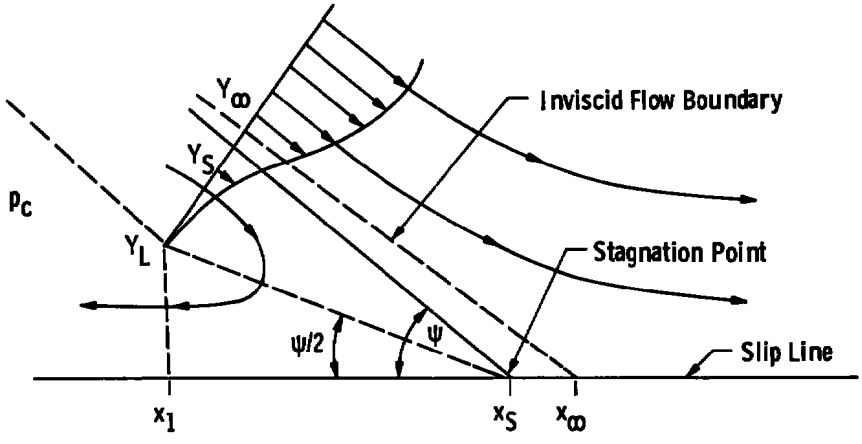

Figure 10. Assumed recompression flow field.

The location of the stagnation point is determined by comparing the values of total pressure for all possible stagnating streamlines with the slip line pressure distribution as illustrated in Fig. 11.

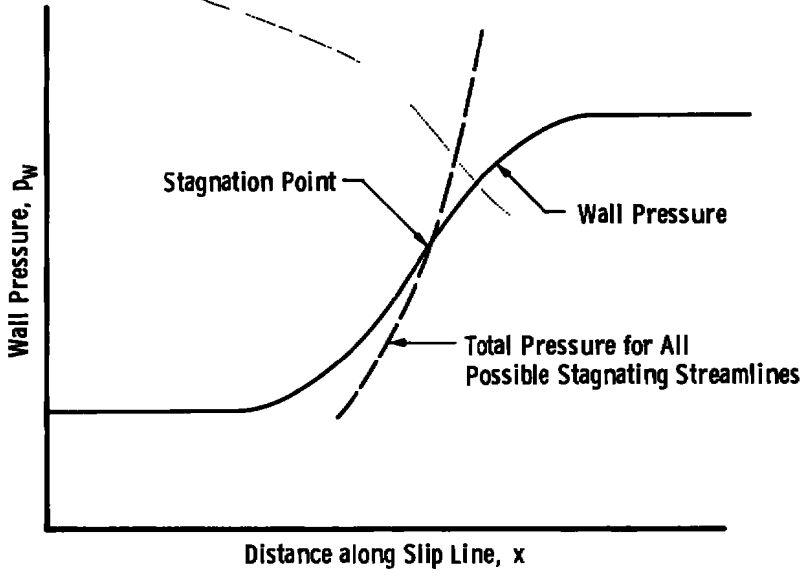

Figure 11. Conditions at stagnation point.

The analysis was applied to the nozzle-afterbody flow shown in Fig. 2 based on the assumption that the slip line, Fig. 2, is a conical surface. The following equations can be derived from the geometry of the jet plume.

$$x_{S_1} = X_\infty - \frac{\ell_1 (\eta_{\infty_1} - \eta_{S_1}) \cos \alpha_1 \cos \omega}{\sigma_1 \sin [\beta_1 + \alpha_1 - \omega]} \left(\frac{1 + R_\infty}{2R_\infty}\right) \tag{79}$$

$$X_{1_1} = X_{S_1} - \frac{\ell_1 (\eta_{S_1} - \eta_{L_1}) \left[\cos \alpha_1 \cos \omega - \left(\frac{X_\infty - X_{S_1}}{\ell_1}\right) \cos (\beta_1 - \omega_1)\right]}{\sigma_1 \left[\frac{(\eta_{S_1} - \eta_{L_1})}{\sigma_1} \left(\frac{1 + R_\infty}{2R_\infty}\right) \cos \alpha_1 + \tan\left(\frac{\beta_1 + \alpha_1 - \omega}{2}\right)\right] \left(\frac{2R_\infty}{1 + R_\infty}\right)} \tag{80}$$

$$X_{2_1} = 2X_\infty - X_{1_1} \tag{81}$$

where

$$\tan \alpha_1 = \left(\frac{\eta_{\infty_1} - \eta_{S_1}}{\sigma_1}\right) \left(\frac{1 + R_\infty}{2R_\infty}\right) \tag{82}$$

The pressure at the stagnation point is given by the following equation from Eq. (77),

$$\frac{p_{S_1}}{p_c} = 1 - \left[\frac{p_3}{p_c} - 1\right] \sin^2 \frac{\pi}{2} \left[\frac{X_{S_1} - X_{1_1}}{X_{2_1} - X_{1_1}}\right] \tag{83}$$

Equations (79) through (83) are evaluated using the properties of the mixing zone located at (X_i, R_i). The only unknown is η_{S_1}, the location of the stagnation point in terms of the mixing coordinates. For an assumed value of η_{S_1} Eqs. (79) through (83) determine the pressure, p_{S_1}, at the corresponding stagnation point. Assuming p_{S_1} is the total pressure of the streamline impinging at η_{S_1}, the velocity ratio, ϕ_{S_1}, can be determined from

$$1 - \left(\frac{p_c}{p_{S_1}}\right)^{\frac{\gamma_{S_1} - 1}{\gamma_{S_1}}} = \frac{\phi_{S_1}^{\,2}}{\left(\frac{C_{p_{S_1}} T_{t_{S_1}}}{C_{p_1} T_{t_1}}\right)} \left[1 - \left(\frac{p_c}{p_{t_1}}\right)^{\frac{\gamma_1 - 1}{\gamma_1}}\right] \tag{84}$$

where

$$\frac{\gamma_{S_1} - 1}{\gamma_{S_1}} = \frac{\left(\frac{R_{g_{S_1}}}{R_{g_1}}\right)}{\left(\frac{C_{p_{S_1}}}{C_{p_1}}\right)} \left(\frac{\gamma_1 - 1}{\gamma_1}\right) \tag{85}$$

The values of $T_{t_{S_1}}/T_{t_1}$, $C_{p_{S_1}}/C_{p_1}$, R_{g_1}/R_{g_1} are functions of ϕ_{S_1} and η_{S_1} defined by Eqs. (7), (8), and (9).

The velocity ratio, ϕ_{S_1}, can also be determined from Eq. (9) in the form

$$\phi_{S_1} = \frac{1}{2}\left[1 + \operatorname{erf}(\eta_{S_1} - \eta_{P_1})\right] + \frac{\eta_{P_1}}{\sqrt{\pi}} \int_0^{1.0} \phi_{i_1} \ell^{-\left[\eta_{S_1} - \eta_{P_1}\left(\frac{y}{\delta_1}\right)\right]^2} d\left(\frac{y}{\delta_1}\right) \tag{86}$$

where

$$\eta_{P_1} = \left(\frac{\sigma}{\ell_1}\right)\left(\frac{\delta_1}{r_1}\right)\left(\frac{2R_\infty}{1 + R_\infty}\right) \tag{87}$$

$$\phi_{i_1} = \left(\frac{y}{\delta_1}\right)^{\frac{1}{n_1}} \tag{88}$$

The stagnation point location is defined when the assumed value of η_{S_1} results in equal values of ϕ_{S_1} from Eqs. (84) and (86).

The recompression of the external stream along the conical slip line (Fig. 2) is computed independent of the recompression of the jet plume. As a result, the location of stagnation point of the external stream may be different, as may be the stagnation pressure, from that of jet plume. Physically, for this to be true, it would be necessary for a secondary vortex system to exist in the recompression zone between the two stagnation points. Since the existence or nonexistence of such a vortex system has not been established, the authors of this report have elected not to impose the single stagnation point condition.

The recompression equations for the external stream are

$$X_{S_2} = X_\infty - \frac{\ell_2(\eta_{\infty_2} - \eta_{S_2}) \cos\omega \cos\alpha_2}{\sigma_2 \sin(\omega - \beta_2 + \alpha_2)} \left(\frac{R_2 + R_\infty}{2R_\infty}\right) \tag{89}$$

$$X_{I_2} = X_{S_2} - \frac{\ell_2(\eta_{S_2} - \eta_{L_2})\left[\cos\alpha_2 \cos\omega - \left(\frac{X_i - X_{S_2}}{\ell_2}\right)\cos(\omega - \beta_2)\right]}{\sigma_2\left[\frac{(\eta_{S_2} - \eta_{L_2})}{\sigma_2}\left(\frac{R_2 + R_\infty}{2R_\infty}\right)\cos\alpha_2 + \tan\left(\frac{\omega - \beta_2 - \alpha_2}{2}\right)\right]}\left(\frac{R_2 + R_\infty}{2R_\infty}\right) \tag{90}$$

$$X_{2_2} = 2X_\infty - X_{1_2} \tag{91}$$

where

$$\tan \alpha_2 = \left(\frac{\eta_{\infty_2} - \eta_{S_2}}{\sigma_2}\right)\left(\frac{R_2 + R_\infty}{2R_\infty}\right) \tag{92}$$

$$\frac{p_{S_2}}{p_c} = 1 - \left[\frac{p_3}{p_c} - 1\right] \sin^2 \frac{\pi}{2} \left[\frac{X_{S_2} - X_{1_1}}{X_{2_2} - X_{1_1}}\right] \tag{93}$$

$$1 - \left(\frac{p_c}{p_{S_2}}\right)^{\frac{\gamma_{S_2} - 1}{\gamma_{S_2}}} = \frac{\phi_{S_2}{}^2}{\left(\frac{C_{p_{S_2}} T_{t_{S_2}}}{C_{p_1} T_{t_1}}\right)} \left[1 - \left[\left(\frac{p_c}{p_{t_1}}\right)\left(\frac{p_{t_1}}{p_{t_2}}\right)\right]^{\frac{\gamma_2 - 1}{\gamma_2}}\right] \tag{94}$$

where

$$\frac{\gamma_{S_2} - 1}{\gamma_{S_2}} = \frac{\left(\frac{R_{g_{S_2}}}{R_{g_2}}\right)}{\left(\frac{C_{p_{S_2}}}{C_{p_2}}\right)} \left(\frac{\gamma_2 - 1}{\gamma_2}\right) \tag{95}$$

$$\phi_{S_2} = \frac{1}{2}\left[1 + \operatorname{erf}(\eta_{S_2} - \eta_{P_2})\right] + \frac{\eta_{P_2}}{\sqrt{\pi}} \int_0^{1.0} \phi_{i_2} \ell^{-\left[\eta_{S_2} - \eta_{P_2}\left(\frac{y}{\delta_2}\right)\right]^2} d\left(\frac{y}{\delta_2}\right) \tag{96}$$

where

$$\eta_{P_2} = \left(\frac{\sigma_2}{\ell_2}\right)\left(\frac{\delta_2}{r_1}\right)\left(\frac{2R_\infty}{R_2 + R_\infty}\right) \tag{97}$$

$$\phi_{i_2} = \left(\frac{y}{\delta_2}\right)^{\frac{1}{n_2}} \tag{98}$$

2.4 SOLUTION CONDITIONS

The mixing and recompression analyses are evaluated based on values of p_c, T_c, R_{g_c}, and C_{p_c}. However, it is not necessary to assume individual values for each of the thermodynamic parameters since they are determined by the mixture equations for the three gases entering the base region. These equations are:

$$\frac{C_{p_c} T_c}{C_{p_1} T_{t_1}} = k_{c_1} + (1 - k_{c_1} - k_{c_E}) \left(\frac{C_{p_2} T_{t_2}}{C_{p_1} T_{t_1}} \right) + k_{c_E} \left(\frac{C_{p_E} T_{t_E}}{C_{p_1} T_{t_1}} \right) \tag{99}$$

$$\frac{C_{p_c}}{C_{p_1}} = k_{c_1} + (1 - k_{c_1} - k_{c_E}) \left(\frac{C_{p_2}}{C_{p_1}} \right) + k_{c_E} \left(\frac{C_{p_E}}{C_{p_1}} \right) \tag{100}$$

$$\frac{R_{g_c}}{R_{g_1}} = k_{c_1} + (1 - k_{c_1} - k_{c_E}) \left(\frac{R_{g_2}}{R_{g_1}} \right) + k_{c_E} \left(\frac{R_{g_E}}{R_{g_1}} \right) \tag{101}$$

and

$$\frac{T_c}{T_{t_1}} = \frac{\text{Eq. (99)}}{\text{Eq. (100)}} \tag{102}$$

These equations utilize the identity

$$k_{c_1} + k_{c_2} + k_{c_E} = 1.0 \tag{103}$$

to eliminate k_{c_2}.

Using Eqs. (99) through (102) requires assuming the three variables p_c, k_{c_1} and k_{c_E} rather than the four variables p_c, T_c, R_c, and C_{p_c}. In addition, for most afterbody flows there is no bleed flow so that only two variables, p_c and k_{c_1} need to be specified. This greatly simplifies the iteration procedure.

For the assumed variables to be a solution the conservation of mass, Eq. (1), must be satisfied and the assumed values of k_{c_1} and k_{c_E} must be equal to the values computed from the equations for conservation of species.

The conservation of mass equation in the transformed plane is

$$k_E \left(\frac{m}{G_1} \right) + \frac{G_2}{G_1} + 1 = 0 \tag{104}$$

where

$$k_E = \frac{m_E}{m_N} \tag{105}$$

$$\frac{G_1}{m_N} = \frac{2\pi r_\infty}{m_N} \int_{Y_{D_1}}^{Y_{S_1}} \rho u dY_1 \tag{106}$$

$$\frac{G_2}{m_N} = \frac{2\pi r_\infty}{m_N} \int_{Y_{D_2}}^{Y_{S_2}} \rho u dY_2 \tag{107}$$

$$\frac{G_2}{G_1} = \left(\frac{\gamma_1 - 1}{\gamma_2 - 1}\right)\left(\frac{\gamma_2}{\gamma_1}\right)\left(\frac{C_2}{C_1}\right)\left[\frac{C_{p_1} T_{t_1}}{C_{p_2} T_{t_2}}\right]^{\frac{1}{2}}\left(\frac{\ell_2}{\ell_1}\right)\left(\frac{\sigma_1}{\sigma_2}\right)\left(\frac{R_2 + R_\infty}{1 + R_\infty}\right)\left(\frac{\Delta I_2}{\Delta I_1}\right) \tag{108}$$

and

$$\frac{m_N}{G_1} = \left(\frac{\sigma_1}{\Delta I_1}\right)\left(\frac{R_\infty}{1 + R_\infty}\right)\left(\frac{R_\infty}{\ell_1}\right)\left(\frac{A^*}{A_N}\right)\left[\frac{2}{\gamma_1 + 1}\right]^{\frac{1}{\gamma_1 - 1}}\left[\frac{\gamma_1 - 1}{\gamma_1 + 1}\right]^{\frac{1}{2}} \frac{(1 - C_1^2)^{-\left(\frac{\gamma_1}{\gamma_1 - 1}\right)}}{C_1} \tag{109}$$

The equations for k_{c_1} and k_{c_E} are derived as follows:

From Fig. 2:

$$k_{c_1} = \frac{2\pi r_\infty \int_{Y_{L_1}}^{Y_{S_1}} k_1 \rho u dY_1}{m_E + 2\pi r_\infty \int_{Y_{L_1}}^{Y_{S_1}} k_1 \rho u dY_1 + 2\pi r_\infty \int_{Y_{L_2}}^{Y_{S_2}} k_2 \rho u dY_2} \tag{110}$$

and

$$k_{c_E} = \frac{m_E}{m_E + 2\pi r_\infty \int_{Y_{L_1}}^{Y_{S_1}} k_1 \rho u dY_1 + 2\pi r_\infty \int_{Y_{L_2}}^{Y_{S_2}} k_2 \rho u dY_2} \tag{111}$$

In the transformed plane, Eqs. (110) and (111) are

$$k_{c_1} = \frac{(I_6)_{\eta_{S_1}}}{k_E\left(\frac{m_N}{G_1}\right)\Delta I_1 + (I_6)_{\eta_{S_1}} + \left(\frac{\ell_2}{\ell_1}\right)\left(\frac{\sigma_1}{\sigma_2}\right)\left(\frac{\rho_2\mu_2}{\rho_1\mu_1}\right)\left(\frac{R_2 - R_i}{1 - R_i}\right)(I_6)_{\eta_{S_2}}} \tag{112}$$

and

$$k_{c_E} = \frac{k_E\left(\frac{m_N}{G_1}\right)\Delta I_1}{k_E\left(\frac{m_N}{G_1}\right)\Delta I_1 + (I_6)_{\eta_{S_1}} + \left(\frac{\ell_2}{\ell_1}\right)\left(\frac{\sigma_1}{\sigma_2}\right)\left(\frac{\rho_2\mu_2}{\rho_1\mu_1}\right)\left(\frac{R_2 + R_i}{1 + R_i}\right)(I_6)_{\eta_{S_2}}} \tag{113}$$

3.0 EVALUATION OF THEORY

The purpose of this evaluation is to establish the general quantitative accuracy of the analytical technique. Evaluation of the various components of the analysis is not possible at this time, since the existing experimental data consist of only base pressure measurements. The experimental data selected for this evaluation are those which show the effects on base pressure of (1) base bleed, (2) thermodynamic properties, (3) initial boundary layers, and (4) geometry.

In the following sections the analysis is compared to experiments having an external stream Mach number of 2.0. The jet Mach number is also 2.0 except for the one hot rocket configuration. These data were selected because the present analysis does not include a method for estimating the change in initial boundary-layer properties caused by the expansion process at the separation point. Many approximate analyses have been developed for this phenomena, Ref. 4, and all show that at Mach 2.0 the momentum thickness of the boundary layer is relatively unaffected by the expansion process.

3.1 DAVIS EXPERIMENT

Davis, Ref. 19, investigated the effect of chemical reactions on base pressure for M = 2.0 flow over a two-dimensional blunt base by injecting hydrogen in the base region and igniting with a pilot flame. Of interest in this report are the data presented in Ref. 19 showing the effect on base pressure of a hydrogen bleed without chemical reactions. Two-dimensional base flow can be simulated by an axisymmetric configuration having a small base height ($r_2 - r_N$), Fig. 2, relative to the jet radius, r_N. Experimental data for an axisymmetric system having $r_2 - r_N/r_N = 1.25$ obtained by Reid and Hastings, Ref. 20, are shown in Fig. 12a to agree well with the Davis two-dimensional value for no bleed. The axisymmetric configuration selected for simulating two-dimensional base flow has a value of $r_2 - r_N/r_N = 1.2$.

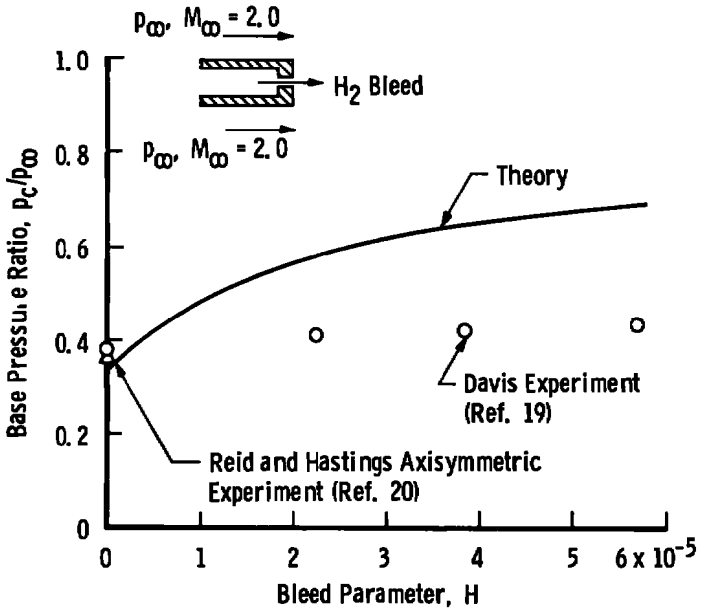

a. Base pressure

Figure 12. Comparison of theory with Davis experiment.

Davis presents his data in terms of a base bleed parameter defined as

$$H = \frac{m_E}{A_c\, p_{t_\infty}} \sqrt{\frac{R_{g_\infty}\, T_{t_\infty}\, (\gamma_\infty - 1)}{2\gamma_\infty}} \tag{114}$$

The analysis in this report requires as input, k_E, the ratio of bleed mass flow to jet mass flow. The two bleed flow parameters are related by

$$k_E = \frac{H}{M_\infty} \left(\frac{A_c}{A_N}\right) \frac{\left(\frac{T_\infty}{T_{t_\infty}}\right)^{\frac{1}{2}}}{\left(\frac{p_\infty}{p_{t_\infty}}\right)} \sqrt{\frac{2}{\gamma_\infty - 1}} \tag{115}$$

For the specific conditions of the Davis experiment

$$k_E = 2.823\, H \tag{116}$$

The theoretical variation of base pressure with bleed flow is compared with experiment in Fig. 12a. The theory agrees well with experiment for no bleed, but is greater than experiment by about 50 percent for the maximum bleed case. This indicates the theoretical rate of mixing is too low, as was previously shown for incompressible mixing in Figs. 3a and 3b.

The theoretical variation of specific heat ratio in the base region is presented in Fig. 12b and shows the expected trend with bleed flow. The variation of the similarity parameter, σ, with bleed flow is shown in Fig. 12c to decrease with increasing bleed flow.

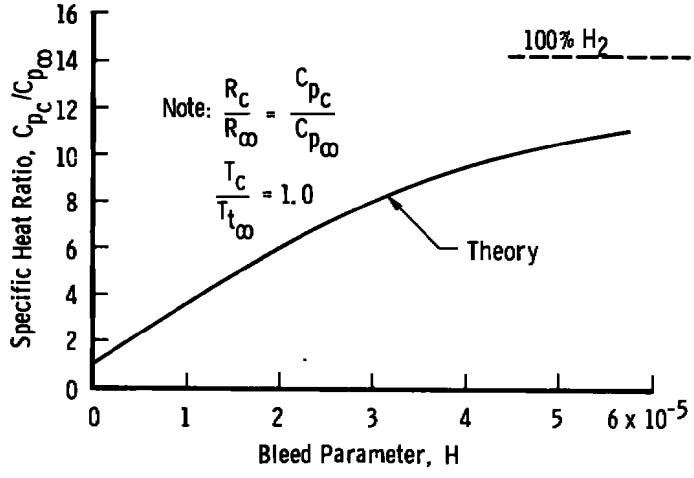

b. Base thermodynamic properties

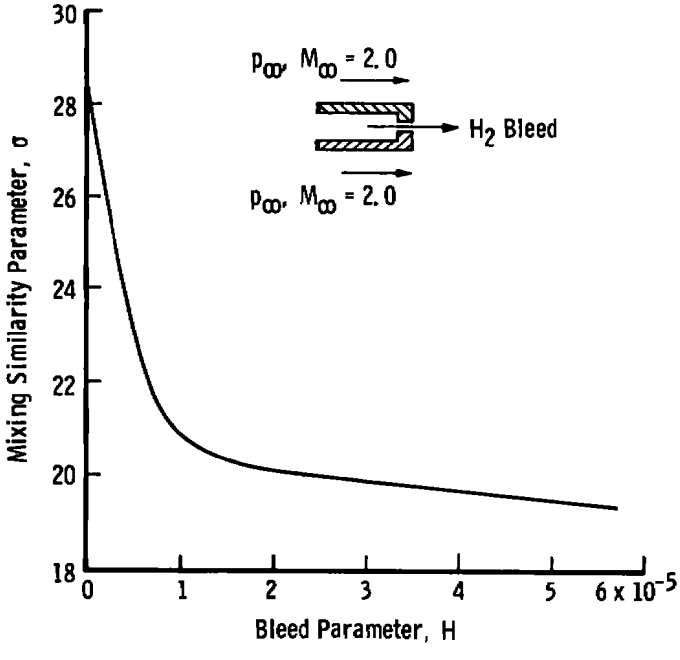

c. Mixing similarity parameter
Figure 12. Continued.

The trend of σ decreasing with H_2 bleed flow is inconsistent with both the Donaldson and Gray and Channapragada formulations for turbulent mixing (Refs. 21 and 22). Finally,

the variation of a Nash-type recompression factor, N, Ref. 4, with bleed flow is presented in Fig. 12d. For no bleed flow the theoretical value of 0.42 agrees well with the value 0.35 assumed by Nash based on experiment. The decrease in the recompression factor, N, with increasing bleed flow is consistent with the experimental results obtained by Carrière and Sirieix, Ref. 23, using air as the bleed gas.

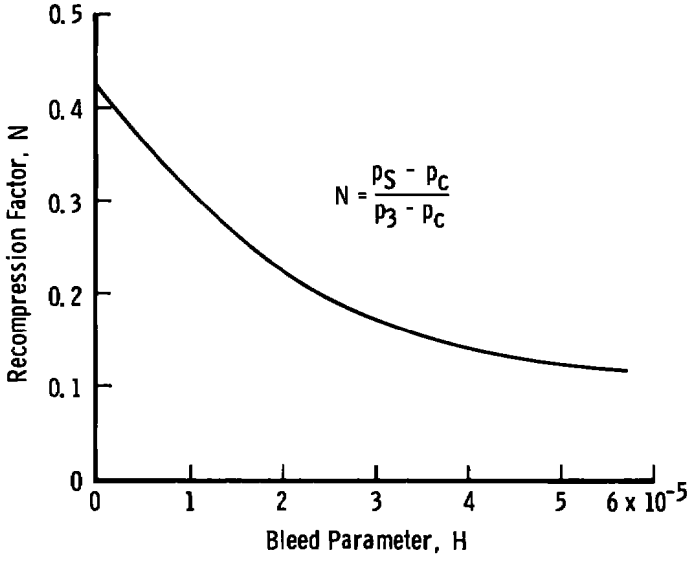

d. Recompression factor
Figure 12. Concluded.

3.2 TWO-DIMENSIONAL BACKWARD-FACING STEP EXPERIMENTS

The theoretical effect of initial boundary-layer momentum thickness on the base pressure for Mach 2.0 flow over a backward-facing step is compared with experiment in Fig. 13a. The theoretical results were obtained for the same axisymmetric configuration used to represent the Davis two-dimensional experiment. The theoretical base pressure is shown in Fig. 13a to agree well with Chow's analysis (Ref. 17) for relatively thin initial boundary layers. and with Alber and Lees analysis for the thicker initial boundary layers. The theoritical base pressure is about 25 percent larger than experiment at the higher values of θ_∞/h. The theoretical mixing similarity parameter, σ, is presented in Fig. 13b as a function of boundary-layer thickness, but its variation is due entirely to the change with base pressure of the inviscid flow Mach number along the edge of the mixing zone. The theoretical variation of a Nash-type recompression factor with initial boundary-layer thickness is presented in Fig. 13c. The magnitude of the recompression factor is in good agreement with that presented by Nash in Ref. 4. In addition, the small variation of the recompression factor with boundary-layer thickness is consistent with the assumption, by Nash, of a constant recompression factor used in his analysis.

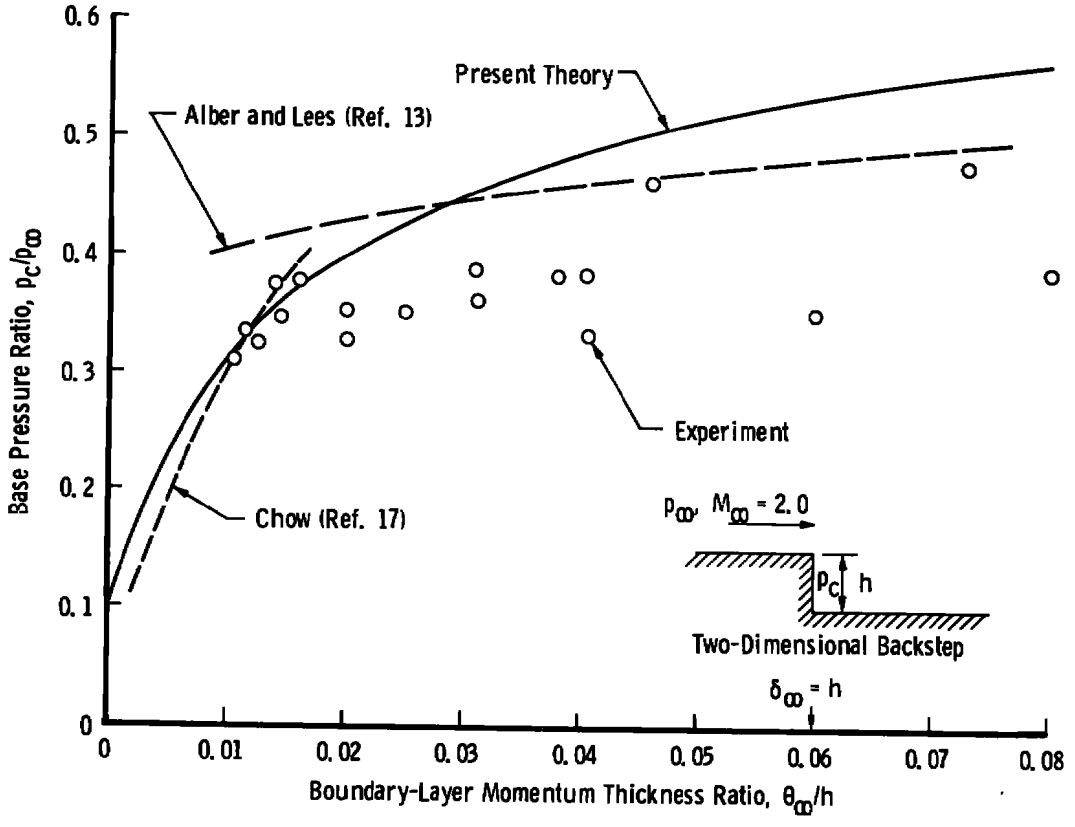

a. Initial boundary-layer effect on base pressure

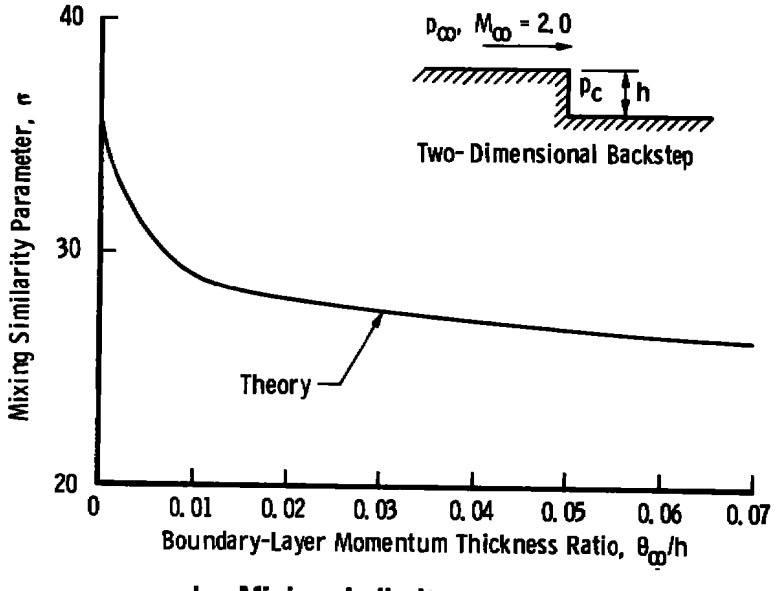

b. Mixing similarity parameter

Figure 13. Comparison of theory with two-dimensional backstep experiment.

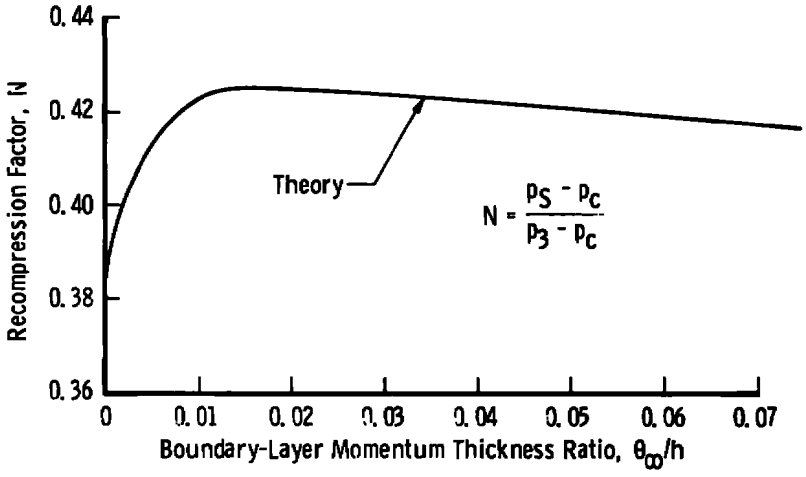

c. Recompression factor
Figure 13. Concluded.

3.3 ROCKET-AFTERBODY CONFIGURATION

The theory was applied to the rocket-afterbody configuration shown in Fig. 14a to determine the effect on base properties of the external stream boundary-layer thickness.

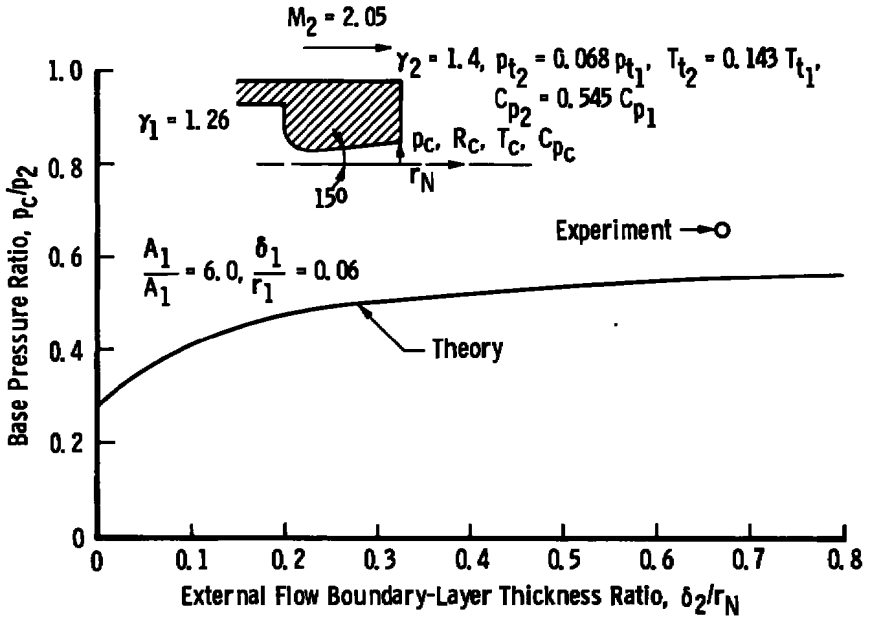

a. Base pressure
Figure 14. Application of theory to a rocket-afterbody configuration.

The theoretical variation in the base pressure shown in Fig. 14a is much less than that computed for the flow over a backward-facing step, Fig. 13a. Apparently the base heating effect for a thin boundary layer, shown in Fig. 14b, prevents the base pressure from decreasing at low values of δ_2.

The variation of the mixing similarity parameter, σ, and the recompression factors for each stream are presented in Figs. 14c and d. The recompression factors are different

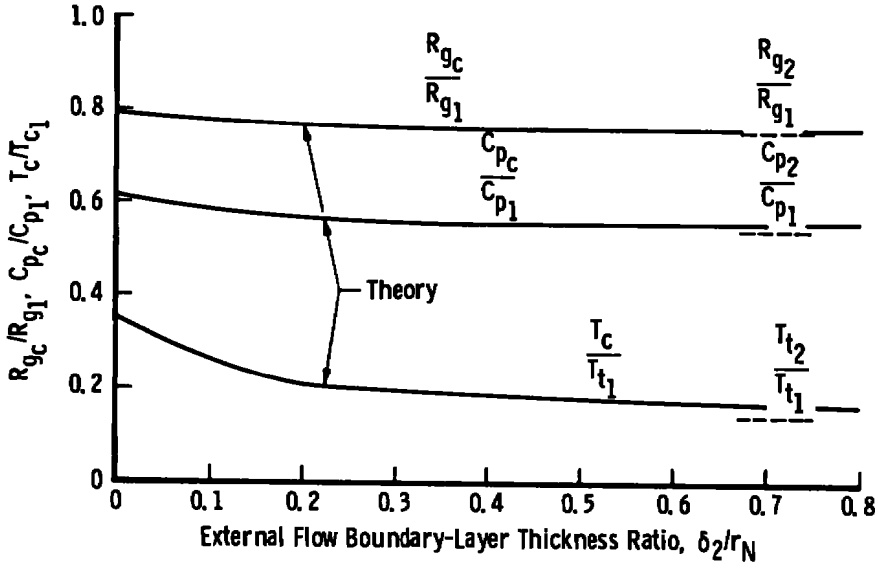

b. Base thermodynamic properties

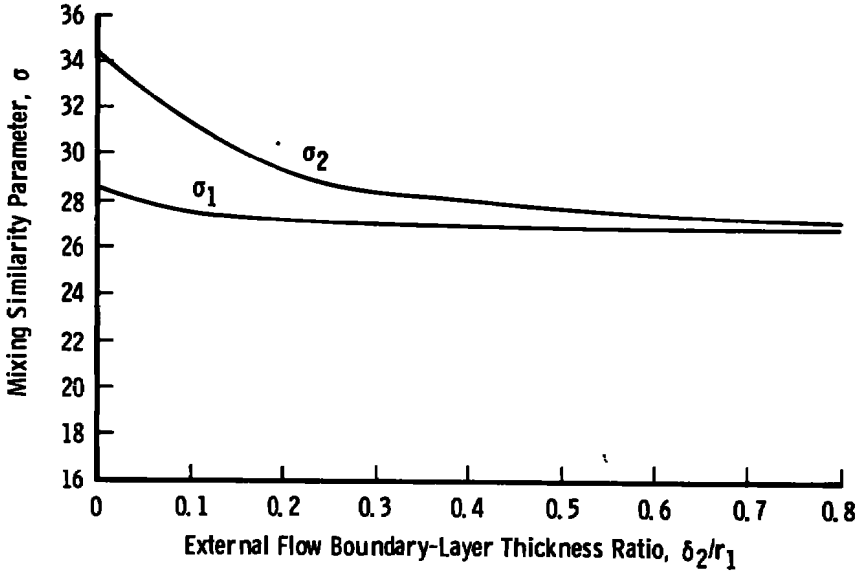

c. Mixing similarity parameters
Figure 14. Continued.

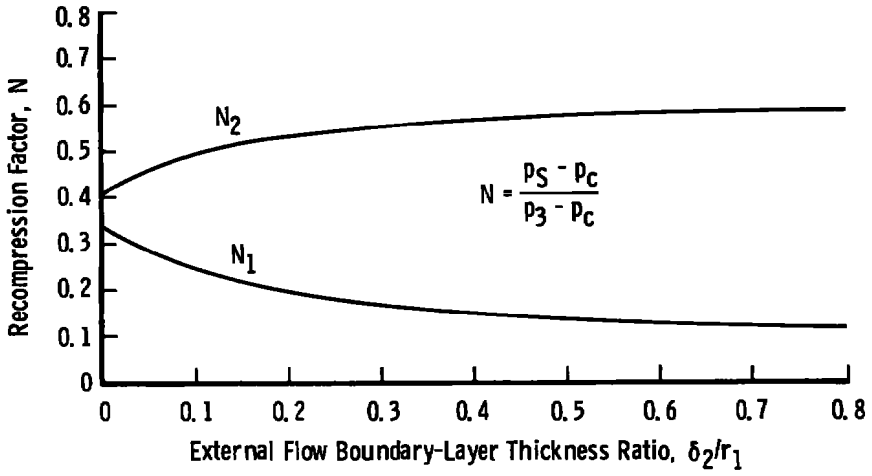

d. Recompression factors
Figure 14. Concluded.

because they are computed independent of each other as previously discussed. The recompression factor, N, indicates the relative location of the stagnating streamline in the mixing zone. For N = 1.0 the stagnating streamline is located in the high-speed portion of the mixing zone. For N = 0 the stagnating streamline is located at the low-speed edge of the mixing zone and the entire mixing zone mass flow will proceed downstream. The recompression factor for the external stream, N_2, is shown in Fig. 14d to increase as the boundary-layer thickness increases, thus reflecting the rejection of more and more of the boundary-layer mass flow into the base region. As a result, the recompression factor for the jet, N_1, is decreasing indicating an increase in the jet pumping capacity.

3.4 REID AND HASTINGS EXPERIMENT

Reid and Hastings, Ref. 20, experimentally studies a family of afterbody geometries, all at an external stream and jet Mach number of 2.0. The most extreme configuration tested had an external surface radius five times the jet radius. The theoretical base pressure as a function of external boundary-layer thickness for that configuration is presented in Fig. 15a. The theoretical base pressure increases significantly with boundary-layer thickness just as it does for flow over a backward-facing step. The theory is about 35 percent greater than the experimental value given by Reid and Hastings. The variation of the recompression factor for each stream is presented in Fig. 15b, and the trend is the same as for the rocket-afterbody configuration previously discussed.

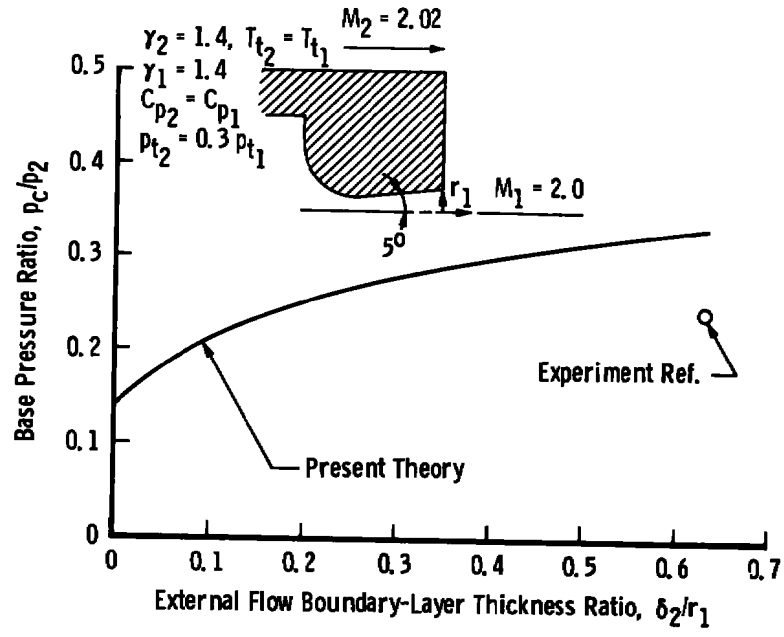

a. Base pressure

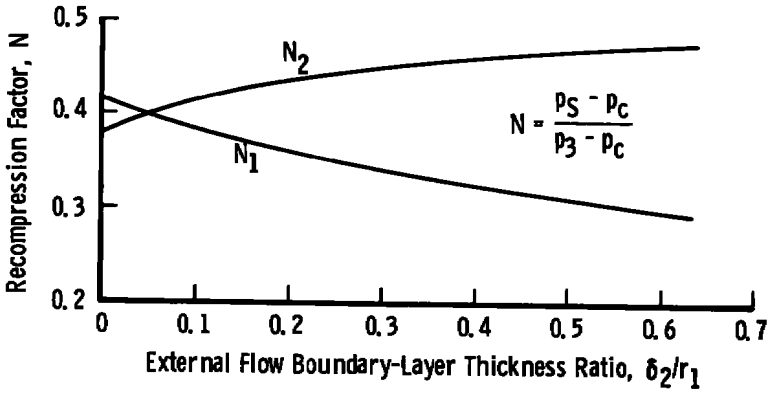

b. Recompression factors

Figure 15. Comparison of theory with Reid and Hastings experiment.

4.0 CONCLUDING REMARKS

The evaluation of the analysis shows that usually the theoretical base pressure is greater than experiment. The experimental data are too limited to indicate which parts of the analysis are most seriously in error. Since the only empiricism used is in the turbulent mixing analysis, this would be the simplest to modify. However, a higher rate of mixing is required to reduce the theoretical base pressure which could be obtained by use of the Donaldson and Gray formulation (Ref. 21) for the turbulent mixing analysis.

REFERENCES

1. Korst, H. H., Chow, W. L., and Zumwalt, G. W. "Research on Transonic and Supersonic Flow of a Real Fluid at Abrupt Increase in Cross Section (with Special Considerations of Base Drag Problems) Final Report." University of Illinois Report No. ME-TR-392-5, University of Illinois, Urbana, Illinois, December 1959.

2. Addy, A. L. "Analysis of the Axisymmetric Base-Pressure and Base-Temperature Problem with Supersonic Interacting Free-stream-Nozzle Flows Based on the Flow Model of Korst, et al., Part II: A Comparison and Correlation with Experiment for Cylindrical Afterbodies." Report No. RD-TR-69-13 (AD868895), U. S. Army Missile Command, Redstone Arsenal, Alabama, December 1969.

3. Fong, M. C., "An Analysis of Plume-Induced Boundary-Layer Separation." Journal of Spacecraft and Rockets, Vol. 8, No. 11, November 1971, pp. 1107-1114.

4. Nash, J. R. "An Analysis of Two-Dimensional Turbulent Base Flow, Including the Effect of the Approaching Boundary Layer." Reports and Memoranda No. 3344, Aeronautical Research Council, Ministry of Aviation, London, Great Britain, July 1962.

5. Carrière, P. and Sirieix, M. "Resultats Recents dans L'Etude des Problems de Melange et de Recollement." ONERA T.P. No. 165, Office National d'Etudes et de Recherches Aerospatiales (ONERA), 29, Avenue de la Division Leclerc, Chatillon-sous-Bagneux (Seine), France, 1964, (also available as: Library Translation No. 1113. May 1965, Royal Aircraft Establishment, Ministry of Aviation, Farnborough, Kants, U.K.)

6. Page, R. H., Kessler, F. J., and Hill, W. G., Jr. "Reattachment of Two-Dimensional Supersonic Turbulent Flows." ASME Paper No. 67-FE-20, presented at ASME Fluids Engineering Conference, Chicago, Illinois, 1967.

7. Sirieix, M., Delery, J., and Mirande, J.. "Recherches Experimentales Fondamentales sur les Ecoulments Separes et Applications." T.P. No. 520, Office National d'Etudes et de Recherches Aerospatiales (ONERA), 29, Avenue de la Division Leclerc-92, Chatillon, France, 1967.

8. Dixon, R. J., Richardson, J. M., and Page, R. H. "Turbulent Base Flow on an Axisymmetric Body with a Single Exhaust Jet." AIAA Paper No. 69-650, presented at AIAA Fluid and Plasma Dynamics Conference, San Francisco, California, June 16-18, 1969.

9. Bauer, R. C. "Theoretical Base Pressure Analysis of Axisymmetric Ejectors without Induced Flow." AEDC-TDR-64-3, January 1964.

10. Bauer, R. C. "Characteristics of Axisymmetric and Two-Dimensional Isoenergetic Jet Mixing Zones." AEDC-TDR-63-253 (AD426116), December 1963.

11. Bauer, R. C. and Matz, R. J. "Influence of Initial Boundary Layer on the Two-Dimensional Turbulent Mixing of a Single Stream." AEDC-TR-71-79 (AD722442), April 1971.

12. Chapman, A. J. "Mixing Characteristics of a Free Jet Boundary with Consideration of Initial Boundary Layer Configuration." Ph.D Thesis, University of Illinois, 1953.

13. Alber, I. E. and Lees, L. "Integral Theory for Supersonic Turbulent Base Flows." AIAA Journal, Vol. 6, No. 7, July 1968.

14. Peters, C. E. and Phares, W. J. "An Integral Turbulent Kinetic Energy Analysis of Free Shear Flows, Free Turbulent Shear Flows, Vol. I." Conference Proceedings, NASA SP 321, 1973, pp. 577-624.

15. Narayanan, M. A. B., Khadgi, Y. N., and Viswanath, P. R. "Similarities in Pressure Distribution in Separated Flow Behind Backward-Facing Steps." Aeronautical Quarterly, November 1974.

16. Viswanath, P. R. and Narasimha, R. "Two-Dimensional Boat-Failed Bases in Supersonic Flow." Aeronautical Quarterly, August 1974.

17. Chow, W. L. "Recompression of a Two-Dimensional Supersonic Turbulent Free Shear Layer." Developments in Mechanics, Vol. 6, Proceedings of the Twelfth Midwestern Mechanics Conference, 1971, pp. 319-331.

18. O'Leary, R. A. and Mueller, F. J. "Correlation of Physical and Numerical Experiments for Incompressible Laminar Separated Flows." University of Notre Dame, Themis-UND-69-4.

19. Davis, L. R. "The Effect of Chemical Reactions in the Turbulent Mixing Component on the Dynamics and Thermodynamics of Wake Flow Fields." Ph.D Thesis, University of Illinois, 1964.

20. Reid, J. and Hastings, R. C. "The Effect of a Central Jet on Base Pressure of a Cylindrical Afterbody in a Supersonic Stream." Report No. Aero 2621, also R&M No. 3224, Royal Aircraft Establishment, Farnborough, England, December 1969.

21. Bauer, R. C. "Another Estimate of the Similarity Parameter for Turbulent Mixing." AIAA Journal, Vol. 6, No. 5, May 1968.

22. Channapragada, R. S. "Compressible Jet Spread Parameters for Mixing Zone Analyses." AIAA Journal, Vol. I, No. 9, September 1963.

23. Carrière, P. and Sirieix, M. "Facteurs d'Influence du Recollement d'un Ecoulement Supersonique." ONERA Memo. Tech. 20, presented at 10th International Congress of Applied Mechanics, Stresa, 1961.

APPENDIX A
DEFINITION OF INTEGRALS

1. $$(I_1)_\eta = \int_{\eta_L}^{\eta} \frac{\phi \, d\eta}{\frac{R_g}{R_{g_\infty}}\left[\frac{T_t}{T_{t_\infty}} - \left(\frac{C_{p_\infty}}{C_p}\right) C_\infty{}^2\phi^2\right]}$$

2. $$(I_2)_\eta = \int_{\eta_L}^{\eta} \frac{\phi^2 \, d\eta}{\frac{R_g}{R_{g_\infty}}\left[\frac{T_t}{T_{t_\infty}} - \left(\frac{C_{p_\infty}}{C_p}\right) C_\infty{}^2\phi^2\right]}$$

3. $$(I_3)_\eta = \int_{\eta_L}^{\eta} \frac{\phi^3 \, d\eta}{\frac{R_g}{R_{g_\infty}}\left[\frac{T_t}{T_{t_\infty}} - \left(\frac{C_{p_\infty}}{C_p}\right) C_\infty{}^2\phi^2\right]}$$

4. $$(I_4)_\eta = \left(\frac{\rho_\infty}{\rho_m}\right)(1 - C_\infty{}^2)\left[(I_2)_o - \frac{1}{2}\left[(I_1)_o - (I_1)_{\eta_D}\right]\right] \int_{\eta_L}^{\eta} \frac{\bar{K}\phi \, d\eta}{\frac{R_g}{R_{g_\infty}}\left[\frac{T_t}{T_{t_\infty}} - \left(\frac{C_{p_\infty}}{C_p}\right) C_\infty{}^2\phi^2\right]}$$

5. $$(I_5)_\eta = \left(\frac{\rho_\infty}{\rho_m}\right)^{3/2}(1 - C_\infty{}^2)^{3/2}\left[(I_2)_o - \frac{1}{2}\left[(I_1)_o - (I_1)_{\eta_D}\right]\right]^{3/2} \int_{\eta_L}^{\eta} \frac{(\bar{K})^{3/2} \, d\eta}{\frac{R_g}{R_{g_\infty}}\left[\frac{T_t}{T_{t_\infty}} - \left(\frac{C_{p_\infty}}{C_p}\right) C_\infty{}^2\phi^2\right]}$$

6. $$(I_6)_\eta = \int_{\eta_{I_1}}^{\eta} \frac{k\,\phi\,d\eta}{\frac{R_g}{R_{g_\infty}}\left[\frac{T_t}{T_{t_\infty}} - \left(\frac{C_{p_\infty}}{C_p}\right) C_\infty{}^2\phi^2\right]}$$

7. $$\Delta I = (I_1)_{\eta_S} - (I_1)_{\eta_D}$$

NOMENCLATURE

A	Area
A^*	Throat area of jet nozzle
a_1	Turbulent kinetic energy constant, Eq. (44)
a_2	Turbulent kinetic energy constant, Eq. (34)
b	Width of mixing zone
C	Crocco number, Eq. (38)
C_p	Specific heat at constant pressure
c	Turbulent kinetic energy constant, Eqs. (61) and (62)
D	Turbulent kinetic energy dissipation per unit volume, Eq. (32)
G	Mass flow between dividing and stagnation streamlines
H	Base bleed flow parameter, Eq. (114)
h	Step height
I	Integrals defined in Appendix A
ΔI	Nondimensional mass flow between dividing and stagnating streamlines, Appendix A
K	Turbulent kinetic energy per unit mass, Eq. (31)
$\overline{K}$	Nondimensional turbulent kinetic energy, Eq. (42)
k	Mass fraction
ℓ	Length of inviscid flow boundary
M	Mach number

m	Mass flow
N	Recompression factor
n	Exponent on initial boundary-layer profile, Eq. (5)
p	Static pressure
p_t	Total pressure
R	Nondimensional radius, r/r_N
R_g	Gas constant
R_i	Nondimensional radius to intersection of inviscid flow boundaries
R_T	Turbulent Reynolds number, Eq. (50)
r	Radius from centerline of jet
r_∞	Radius to intersection of inviscid flow boundaries
T	Static temperature
T_t	Total temperature
u	Velocity
X	Nondimensional distance from jet exit plane, (x/r_N)
X_∞	Nondimensional distance to intersection of inviscid flow boundaries
X_1	Nondimensional distance to beginning of recompression zone
X_2	Nondimensional distance to peak pressure in recompression zone
x	Distance
x_∞	Distance to intersection of inviscid flow boundaries

x_1	Distance to beginning of recompression region
x_2	Distance to peak pressure in recompression zone
x^*	Distance to average pressure in recompression zone
Y	Mixing zone ordinate, + to high-speed side
y	Initial boundary-layer ordinate
α	Angle between inviscid flow boundary and stagnation streamline, Eqs. (82) and (92)
β	Angle between inviscid flow boundary at (x_∞, r_∞) relative to jet centerline
γ	Ratio of specific heats
δ	Boundary-layer thickness
δ^*	Boundary-layer displacement thickness, Eq. (28)
ϵ	Eddy viscosity
η	Nondimensional mixing zone ordinate, $\sigma Y/x$
η_p	Mixing zone velocity profile shape parameter, Eq. (4)
η_b	Nondimensional width of mixing zone, Eq. (33)
θ	Boundary-layer momentum thickness, Eq. (29)
ρ	Density
σ	Similarity parameter for planar, two-dimensional turbulent mixing
σ_A	Similarity parameter for axisymmetric turbulent mixing
τ	Shear stress

ϕ Nondimensional velocity, u/u_∞

ψ Angle between stagnation streamline and the slip line at x_S, Fig. 10

ω Slip-line angle relative to jet centerline

SUBSCRIPTS

c. Base region

D Dividing streamline

E Bleed flow

i Initial conditions

L Low-speed edge of mixing zone

m Conditions in mixing zone at $\phi = 1/2$

N Jet nozzle

P Position

S Stagnation point

U High-speed edge of mixing zone

1 Jet flow

2 External flow

3 End of recompression region

∞ Inviscid free stream